Main changes are listed as below:

1. The title is changed, as suggested by Albert Ansmann. ‘Stratospheric’ and ‘lower stratosphere’ are used to specify the altitude of the smoke layers in this study.
2. The abstract is rewritten
3. The introduction and conclusion are re-shaped.
4. Figure 11 in the discussion manuscript has been removed, and we also removed the argument about particle depolarization ratio increasing with transport time. More efforts are needed in investigating CALIOP data and their uncertainty before drawing convincing conclusions. This work is planned for the next step.
5. The error estimation part is moved in the Appendix
6. Discussion about the error of molecular scattering in the optical thickness is added
7. The methodology is now presented before the observations
8. The PLDR355 nm on 31 August is corrected to 0.28±0.08 (error recalculated)
9. More information about GARRLiC/GRASP algorithm is added.
10. Comments about the error of regularization inversion are discussed.
11. The error of Klett method is discussed. A comparison of backscatter coefficient between Klett and Raman is shown in the response file, showing that Klett can provide very consistent backscatter coefficient profile, which justifies the application of Klett method in this study.
12. Discussion section is reshaped and polished.
13. Table 1 is added to summarize the three Lidar systems
14. Figure 2 is added to illustrate the ascent of the smoke plume when exposed to sunlight
15. Smoke layer thickness, mean extinction coefficients are added in Table 2
16. Figure 10 in the discussion version is removed because materials are enough to show the origin of the smoke.
17. The unit of PLDR is changed from % to unitless, to avoid confusion with relative error.
18. ‘Author contribution’ is added and ‘Data availability’ is implemented.

This is a revised manuscript responding to all the four reviews.
The paragraphs in red in this manuscript are modifications corresponding to the response to the four reviews.
Different colors refer to different reviewers
And the numbers coincide with the ones in the response file, which was uploaded as supplement on 16 Nov 2018.

Anonymous Referee #1: AR1 A#. Page 35-37
Anonymous Referee #2: AR2 A#. Page 38-42
Anonymous Referee #3: AR3 A#. Page 43-49
Albert Ansmann: AA A#. Page 50-68

Long-range transported Canadian smoke plumes in the lower stratosphere over northern France

Reply to: AA A1

Qiaoyun Hu[1], Philippe Goloub[1], Igor Veselovskii[2], Juan-Antonio Bravo Aranda[3], Ioana Popovici[1,4], Thierry Podvin[1], Martial Haeffelin[3], Anton Lopatin[5], Christophe Pietras[3], Xin Huang[5], Benjamin Torres[1], and Cheng Chen[1]

[1]Univ. Lille, CNRS, UMR8518 – LOA – Laboratoire d'Optique Atmosphérique, 59000 Lille, France
[2]Physics Instrumentation Center of GPI, Troitsk, Moscow, 142190, Russia
[3]Institut Pierre Simon Laplace, École Polytechnique, CNRS, Université Paris-Saclay, 91128 Palaiseau, France
[4]CIMEL Electronique, 75011 Paris, France
[5]GRASP-SAS, Remote sensing developments, 59650 Villeneuve d'Ascq, France

Correspondence: Qiaoyun Hu (qiaoyun.hu@univ-lille.fr)

Abstract. Long-range transported Canadian smoke layers in the stratosphere over northern France were detected by three Lidar systems in August 2017. The peaked optical depth of the stratospheric smoke layer exceeded 0.20 at 532 nm, which is comparable with the simultaneous tropospheric aerosol optical depth. The measurements of satellite sensors revealed that the observed stratospheric smoke plumes were transported from Canadian wildfires after being lofted by strong pyro-cumulonimbus. Case studies in two observation site, Lille (50.612°N, 3.142°E, 60 m a.s.l) and Palaiseau (48.712°N, 2.215°E, 156 m a.s.l), are presented in detail. Smoke particle depolarization ratios are measured at three wavelengths: over 0.20 at 355 nm, 0.18–0.19 at 532 nm and 0.04–0.05 at 1064 nm. The high depolarization ratios and its interesting spectral dependence are possibly caused by the irregular-shaped aged smoke particles or/and the mixing with dust particles. Similar results are found by several European Lidar stations and an explanation that can fully resolve this question is not yet found. Aerosol inversion based on Lidar $2\alpha+3\beta$ data derived smoke effective radius about 0.33 μm for both cases. The retrieved single scattering albedo is in the range of 0.8 to 0.9, indicating that the smoke plumes are absorbing. The absorption can cause perturbations to the temperature vertical profile, as observed by ground-based radiosonde, and it is also related to the ascent of the smoke plumes when exposed in sunlight. A direct radiative forcing calculation is performed using the obtained optical and microphysical properties. The calculation revealed that the smoke plumes in the stratosphere can significantly reduce the radiation arriving at the surface, and the heating

rate of the plumes is about 3.5 K per day.

Reply To: The abstract has been rewritten, refer to AR3 **A1.** AR3 **A4.** AA **A2.**

1 Introduction

Stratospheric aerosols play an important role in the global radiative budget and chemistry-climate coupling (Deshler, 2008; Kremser et al., 2016; Shepherd, 2007). Volcanic eruption is a significant contributor of stratospheric aerosols because the explosive force could be sufficient enough to penetrate the tropopause, which is regarded as a barrier to the convection between the troposphere and stratosphere. Besides volcanic eruption, biomass burning has been reported to be one important constituent of the increasing stratospheric aerosols (Hofmann et al., 2009; Khaykin et al., 2017; Zuev et al., 2017). The pyro-cumulonimbus clouds generated in intense fire activities have the potential to elevate fire emissions from the planetary boundary layer to the stratosphere (Luderer et al., 2006; Trentmann et al., 2006). Stratospheric smoke plumes have been reported in many previous studies (Fromm et al., 2000; Fromm and Servranckx, 2003; Fromm et al., 2005; Sugimoto et al., 2010).

In the summer of 2017, intense wildfires spread in the west and north of Canada. By mid-August, the burnt area had grown to almost 9000 km^2 in British Columbia, which broke the record set in 1958 (see the link). The severe wildfires generatedstrong pyro-cumulonimbus clouds, which were recorded by the satellite imaginary MODIS (Moderate Resolution Imaging Spectrometer). The GOES-15 (Geostationary Operational Environmental Satellite) detected five pyro-cumulonimbus clouds in British Columbia on 12 August 2017 (see https://pyrocb.ssec.wisc.edu). Smoke plumes in the troposphere and lower stratosphere were observed by several European Lidar stations in August and September 2017. Ansmann et al. (2018) and Haarig et al. (2018) observed stratospheric and tropospheric smoke layers originated from Canadian wildfires on 21–23 August 2017 in Leipzig, Germany. The maximum extinction coefficient of the smoke layers reached 0.5 km^{-1}, about 20 times higher than the observation 10 months after the eruption of Pinatubo volcano in 1991(Ansmann et al., 1997). Khaykin et al. (2018) reported Canadian smoke layers in the stratosphere over southern France in August 2017 and they found that the stratospheric smoke plumes can travel the whole globe (at middlelatitudes) in about three weeks.

Reoccurring aerosol layers in the troposphere and lower stratosphere were detected by the Lidar systems in northern France during 19 August and 12 September 2017. In this study, we present the stratospheric smoke observations from two French Lidar stations: Lille (50.612°N, 3.142°E, 60 m a.s.l) and Palaiseau (48.712°N, 2.215°E, 156 m a.s.l), and a mobile Lidar system. Satellite measurements from multiple sensors, including UVAI (Ultraviolet aerosol index) from the OMPS NM (Ozone Mapping and Profiler Suite, Nadir Mapper), CO (carbon monoxide) concentration from AIRS (Atmospheric Infrared Sounder), backscatter coefficient and depolarization ratio profiles from CALIPSO (Cloud-Aerosol Lidar and Infrared Pathfinder Satellite Observations) help identify the source and the transport pathway of the smoke layers. This study is focused on the retrieval of the aerosol optical and microphysical properties using Lidar measurements. Further, the radiative effect of the smoke layer is presented.

Reply To: The introduction has been modified as suggested by AR3 **supplement.** , AR3 **A2.** , AR3 **A3.** , AA **A4.** , AA **A11.**

2 Methodology

Reply To: The observations are put after the methodology, refer to AA **A6.**, AA **A13, A16.**

2.1 Lidar data processing

In this subsection, we present the method for processing Lidar measurements and the error estimation is presented in the Appendix. Raman Lidar technique (Ansmann et al., 1992) allows an independent calculation of extinction and backscatter coefficients. When the nitrogen Raman signal is not available, Klett method (Klett, 1985) is used to calculate the extinction and backscatter coefficient, based on an assumption of aerosol Lidar ratio. In this study, the stratospheric aerosol layers are at high altitudes where the signal-to-noise ratio of Raman channels is not sufficient to obtain high quality extinction profile, therefore, we choose Klett method. To reduce the dependence of Klett inversion on the assumption of Lidar ratio, we use a pre-calculated optical depth of the stratospheric aerosol layer as an additional constraint. We test a series of Lidar ratios in the range of 10–120 sr, and apply independent Klett inversion with each Lidar ratio at a step of 0.5 sr. The integral of the extinction coefficient over the stratospheric layer, expressed below, is compared with the pre-calculated optical depth.

$$\tau^i(\lambda) = \int_{r_{base}}^{r_{top}} \alpha_a(\lambda, r) dr \tag{1}$$

where τ^i is the integral of extinction coefficient α_a, derived from Klett inversion. r is the distance, the subscripts *top* and *base* represent the top and and base of the stratospheric aerosol layer,and λ is the Lidar wavelength.

The pre-calculated optical depth is derived from the elastic channel at 355 and 532 nm. The method is widely used in cirrus clouds studies (Platt, 1973; Young, 1995). By comparing the lidar signal with the molecular backscattered lidar signal, we found there is only molecular scattering below and above the smoke plumes. So we can calculate the optical depth of the smoke plumes as below:

Reply To: AA **A18.**

$$\tau^u(\lambda) = \frac{1}{2}\, ln \frac{\overline{P}_{base}(\lambda)\, r_{base}^2\, \beta_m(\lambda, r_{top})}{\overline{P}_{top}(\lambda)\, r_{top}^2\, \beta_m(\lambda, r_{base})} - \int_{r_{base}}^{r_{top}} \alpha_m(\lambda, r) dr \tag{2}$$

where τ^u is the optical depth of the stratospheric smoke layers. $\overline{P}_{top}$ and $\overline{P}_{base}$ represent the mean Lidar signal at the top and the base of the stratospheric layer. α_m and β_m are the molecular extinction an backscatter coefficient. We calculate the lidar

signal mean within a window of 0.5 km at the top and the base of the aerosol layer, to get $\overline{P}(r_{top}, \lambda)$ and $\overline{P}(r_{base}, \lambda)$. We use this method to estimate the optical depth of the stratospheric layer for LILAS and IPRAL measurements. The Lidar ratio leading to the best agreement of τ^i and τ^u is accepted as the retrieved Lidar ratio of the stratospheric aerosol layer. We apply Klett inversion only to the stratospheric aerosol layer, from 1 km below the layer base to 1 km above the layer top. Therefore, the impact of tropospheric aerosols is excluded. Compared to Raman method, the extinction and backscatter coefficients calculated from Klett method are not independent because of the assumed vertically constant aerosol lidar ratio. But in this study, the smoke particles are well mixed, so the vertical variation of lidar ratio is expected to be not significant. Additionally, using Klett method avoids the effects of vertical smoothing that occur to the Raman derived extinction profile.

Reply To: AA **A17.**

The particle linear depolarization ratio, δ_p, is written as:

$$\delta_p = \frac{R\delta_v(\delta_m + 1) - \delta_m(\delta_v + 1)}{R(\delta_m + 1) - (\delta_v + 1)} \tag{3}$$

where R is the backscatter ratio, δ_v is the volume linear depolarization ratio and δ_m is the molecular depolarization ratio. R is defined as the ratio of the total backscatter coefficient to the molecular backscatter coefficient. $\delta_m = 0.004$ is used in the calculation of particle linear depolarization ratio. δ_v is the ratio of the perpendicularly backscattered signal to the parallel backscattered signal, multiplied by a calibration coefficient. The depolarization calibration is designed to calibrate the electro-optical ratio between the perpendicular and parallel channel and is performed following the procedure proposed by Freudenthaler et al. (2009). The particle linear depolarization ratio is a parameter related to the shape of aerosol particles, and it is usually used in the Lidar community for aerosol typing. The particle linear depolarization ratio of spherical particles is zero. For irregular-shaped particles, for example ice particles in cirrus clouds, the measured particle linear depolarization is about 0.40 (Sassen et al., 1985; Veselovskii et al., 2017).

Reply To: AR3 **A6.**

2.2 Aerosol inversion and radiative forcing estimation

The $3\beta + 2\alpha$ from Lidar observations can be inverted to obtain particle microphysical parameters. The regularization algorithm is used to retrieve size distribution, wavelength-independent complex refractive indices, particle number, surface and volume concentrations (Müller et al., 1999; Veselovskii et al., 2002). We apply GRASP (Generalized Retrieval of Aerosol and Surface Properties) to calculate the DRF (Direct Radiative Forcing) effect of the stratospheric aerosol layer. GRASP is the first unified algorithm developed for characterizing atmospheric properties gathered from a variety of remote sensing observations. Depending on the input data, GRASP can retrieve columnar, vertically resolved aerosol properties and surface reflectance

(Dubovik et al., 2014). As a branch of GRASP algorithm, GARRLiC (Generalized Aerosol Retrieval from Radiometer and Lidar Combined data, called GARRLiC/GRASP hereafter) algorithm was developed for the inversion of coincident single- or multi-wavelength Lidar and sun photometer measurements (Lopatin et al., 2013; Bovchaliuk et al., 2016). The two main modules of GARRLiC/GRASP are the forward model and numerical inversion module. The forward module simulates the atmospheric radiation by using radiative transfer and by accounting for the interaction between light and trace gases, aerosols and underlying surfaces. The aerosol scattering properties in the atmosphere are represented by 1 or 2 aerosol components, whose optical properties can be described using a mixture of spheres and spheroids and are vertically independent. The vertically resolved optical properties, such as the extinction and backscatter coefficients etc., measured by Lidar, are described by varying the aerosol vertical concentration. The forward model includes a radiative transfer model in order to simulate multiple types of observations. The radiative transfer equation in GARRLiC/GRASP is solved using this parallel plane approximation. The atmosphere is divided into a series of parallel planes and the optical properties of each parallel plane can be represented by the input parameters. The radiative transfer model is based on the study of Lenoble et al. (2007). The numerical inversion module follows the multi-term least squares method strategy and derives several groups of unknown parameters that fit the observations.

In this study, we apply the forward model of GARRLiC/GRASP to estimate the forcing effect of the observed stratospheric plume in contrast to a standard Rayleigh atmosphere. The input parameters for DRF are the retrieved aerosol microphysical properties from regularization algorithm, including the size distribution, the complex refractive indices as well as the assumed sphere fraction; the aerosol vertical distribution of the stratospheric plume and surface BRDF (Bidirectional Reflectance Distribution Function) parameters. The forward model of GARRLiC/GRASP can produce downward and upward broadband flux, covering the 0.2–4.0 μm spectrum, at vertical levels specified by the users. Hence, we can calculate the DRF and the heating rate specific to smoke plume.

Reply To: AR1 **A4.** AR3 **A7.**

3 Ground-based and satellite observations

3.1 Simultaneous Lidar and sun photometer observations

LILAS (**LI**lle **L**idar **A**tmospheric **S**tudy) is a multi-wavelength Raman Lidar (Bovchaliuk et al., 2016; Veselovskii et al., 2016) operated at LOA (Laboratoire d'Optique Atmosphérique, Lille, France). LILAS system is transportable and has three elastic channels (355, 532 and 1064 nm), with the capability of measuring the depolarization ratios at these wavelengths. Further it has three Raman channels at 387, 408 and 530 nm. IPRAL system (**IP**SL Hi-Performance multi-wavelength **RA**man **L**idar, Bravo-Aranda et al. (2016); Haeffelin et al. (2005)) is a multi-wavelength Raman Lidar operated at SIRTA (Site Instrumental de Recherche par Télédétection Atmosphérique, Palaiseau, France). The distance between the two systems is around 300 km. Lidar IPRAL has the same elastic channels with LILAS, but the three Raman channels are 387, 408 and 607 nm. In IPRAL system, the depolarization ratio is only measured at 355 nm. The two Lidar systems were operated independently and both observed reoccurring smoke layers in the lower stratosphere during the period of 19 August to 12 September 2017. In addition,

sun photometer measurements are available at Lille and Palaiseau, which are both affiliated stations of AERONET (Aerosol Robotic Network). LILAS and IPRAL Lidar systems are affiliated to EARLINET (European Aerosol Research Lidar Network) (Bösenberg et al., 2003; Böckmann et al., 2004; Matthais et al., 2004; Papayannis et al., 2008; Pappalardo et al., 2014). Both systems perform regular measurements and follow the standard EARLINET data quality check and calibration procedures (Freudenthaler et al., 2018).

On 29 August, three Lidar systems in northern France simultaneously observed a stratospheric aerosol layer. The three Lidar systems are LILAS, IPRAL and a single wavelength (532 nm) CIMEL micro-pulse Lidar, which is set up in a light mobile system, MAMS (Mobile Aerosol Monitoring System, Popovici et al. (2018)) to explore aerosol spatial variability. MAMS was traveling between Palaiseau and Lille on 28 and 29 August. MAMS is equipped with a mobile sun photometer, PLASMA (**P**hotomètre **L**éger **A**éroporté pour la **S**urveillance des **M**asses d'**A**ir, Karol et al. (2013)), capable to measure columnar aerosol optical depth (AOD) along the route. The configuration of the three Lidar systems is summarized in Table 1.

Reply To: AA **A5.**

Figure 1 shows the normalized Lidar range-corrected signals and columnar AOD at 532 nm derived from sun photometer measurements on 29 August 2017. The aerosol layers in the lower stratosphere, stretching from 16 to 20 km, were detected by the three Lidars. The IPRAL Lidar system in Palaiseau detected the aerosol layer in the range of 16–20 km on 29 August. The columnar AOD showed no significant variations, staying between 0.30 and 0.40, from 1000 UTC to 1600 UTC and started decreasing from 1700 UTC. Along the route Palaiseau-Lille, MAMS Lidar observed a layer between 16 and 20 km consisting of two well-separated layers. The columnar AOD was very stable, around 0.40, all along the route from Palaiseau to Lille. Lidar LILAS in Lille observed a shallow layer between 18–20 km at about 0800 UTC on 29 August. The thickness of the layer increased to 4 km until 1600 UTC. The columnar AOD increased from 0.20 to 0.40 from 0800 UTC to 1400 UTC. The lidar quicklook indicated that the aerosol content in the lower troposphere did not show significant variations during 0800 UTC and 1200 UTC, so the increased optical depth, 0.2, came mainly from the contribution of the stratospheric aerosol layer.

Figure 2 shows the Lidar range corrected signal at 1064 nm on 24–25 August 2017. The plume between 17 and 18.5 km is the smoke layer. Due to cirrus clouds and low clouds in the troposphere, the lidar signals in the plume are interrupted. In nighttime, the plume base is stable at about 17 km. Just starting from the sunrise time at 04:51 UTC, a gradual and obvious ascent is observed. In 3–4 hours, the plume base ascended about 0.6 km. Between 10:00–16:00 UTC, the plume base stayed stable. The ascent of smoke plume was also presented in Ansmann et al. (2018) and Khaykin et al. (2018). Khaykin et al. (2018) mentioned that the plume ascended very fast during the first few days after being injected into the troposphere. Based on the observation in Figure 2, we derived the ascent rate of approximately 2.1–2.8 km per day, considering that the sunshine duration is 13 hours (according to the latitude of Lille site) and that the vertical speed of the plume is constant. Ansmann et al. (2018) explained that the ascent of the plume may be related to the absorption of soot-containing aerosols and the wind velocity in the stratosphere. Figure 2 shows that the plume does not continuously ascend in the daytime. One possible explanation we infer is that the self-heating and the wind shear reached an equilibrium point in the plume, so it moved neither upward nor downward.

Reply To: AR1 **A.** , AR2 **A.** , AR3 **A.** , AA **A.** , one figure of lidar observation is added, to illustrate the ascent of the plume.

3.2 Radiosonde measurements

We take the radiosonde measurements from two stations closest to the Lidar sites: Trappes (48.77°N, 1.99°E, France) and Beauvechain (50.78°N, 4.76°E, Belgium). Trappes is about 20 km to Palaiseau and Beauvechain is 120 km to Lille. Considering the large spatial distribution of the stratospheric aerosols, it is obvious that the radiosonde passed through this stratospheric smoke layer. Figure 3 shows the temperature at 0000, 1200 UTC, 29 August for Trappes and 2100 UTC, 29 August for Beauvechain. To compare, we plot the temperature profile of Trappes at 1200 UTC, 21 August, when no stratospheric aerosol layers presented. The temperature profiles show clearly an enhancement between 16 and 20 km, which coincides with the altitude at which the stratospheric plumes appear. The spatial-temporal occurrence of this temperature enhancement and the stratosphere plume in two independent stations indicate that they are directly correlated. Fromm et al. (2005, 2008) also presented temperature increase in the stratospheric smoke layers.

Reply To: AR3 **A10.**

3.3 MODIS measurements

MODIS is a key instrument onboard the Terra and Aqua satellites. Terra MODIS and Aqua MODIS are viewing the entire Earth's surface every 1 to 2 days. Several episodes of Canadian wildfires have been observed by MODIS since early July 2017. On 12 August, MODIS observed a thick, grey plume arising from the British Columbia in the west of Canada (not shown, please see the webpage of WorldView: https://worldview.earthdata.nasa.gov). Figure 4 shows the Earth's true color image overlaid with the fires and thermal anomalies on 15 August 2017 when the plumes have spread over a large area. The region marked with the green dashed line is a huge visible smoke plume and in its southwest, MODIS detected a belt of fire spots. Additionally, during the week of 13–19 August, MODIS (see WorldView) observed a widespread cloud coverage over Canada and showed that clouds layers were overshadowed by the smoke plumes, meaning that the plumes were lofted above the cloud layers, as shown in Figure 4.

3.4 OMPS NM UVAI maps

UVAI is a widely used parameter in characterizing UV-absorbing aerosols, such as desert dust, carbonaceous aerosols coming from anthropogenic biomass burning, wildfires and volcanic ash. The UVAI is determined using the 340 and 380 nm wavelength

channels and is defined as:

$$UVAI = -100 \times \left\{ \log_{10} \left[\frac{I_{340}}{I_{380}} \right]_{meas} - \log_{10} \left[\frac{I_{340}}{I_{380}} \right]_{calc} \right\} \quad (4)$$

where I_{340} and I_{380} are the backscattered radiance at 340 and 380 nm channel. The subscript $meas$ represents the measurements and the $calc$ represents the calculation using a radiative transfer model for pure Rayleigh atmosphere. The UVAI is defined so that positive values correspond to UV-absorbing aerosols and negative values correspond to non-absorbing aerosols (Hsu et al., 1999). The OMPS NM onboard the Suomi NPP (National Polar-orbiting Partnership) is designed to measure the total column ozone using backscattered UV radiation between 300–380 nm. A 110° field-of-view (FOV) telescope enables full daily global coverage (McPeters et al., 2000; Seftor et al., 2014). Figure 5 shows the evolution of UVAI from OMPS NM (Jaross, 2017) every two days during 11 and 29 August 2017. The evolution of the UVAI during this event has also been shown in the study of Khaykin et al. (2018). A plume with relatively high UVAI first occurred over British Columbia on 11 August, and the intensity of the plume was moderate. An obvious increase of UVAI from 11 August to 13 August was observed over the north-west of Canada. It is a clear indication that the events on 12 August was responsible for the increase of UVAI. From 13 to 17 August, the plume spread in the northwest-southeast direction and the UVAI in the centre of the plume reached 10. On 19 August, the plume centre reached the Labrador Sea and the forefront of the plume reached Europe. From 21 to 29 August, the UVAI in the map was much lower than the previous week. During this period, we can still distinguish a plume propagating eastward from the Atlantic to Europe, with the UVAI damping during the transport. Figure 5(e)–(f) show that Europe was overshadowed by the high-UVAI plume during 19 and 29 August.

Reply To: AA **A9, A10.** ,

3.5 AIRS CO maps

AIRS is a continuously operating cross-track scanning sounder onboard NASA's Aqua satellite launched in May 2002. AIRS covers the 3.7 to 16 μm spectral range with 2378 channels and a 13.5 km nadir FOV (Susskind et al., 2014; Kahn et al., 2014). The daily coverage of AIRS is about 70% of the globe. AIRS is designed to measure the water vapor and temperature profiles. It includes the spectral features of the key carbon trace gases, CO_2, CH_4 and CO (Haskins and Kaplan, 1992). The current CO product from AIRS is very mature because the spectral signature is strong and the interference of water vapour is relatively low (McMillan et al., 2005). CO, as a product of the burning process, can be taken as a tracer of biomass burning aerosols (Andreae et al., 1988) due to its relatively long lifetime of 1/2 to 3 months. CO can also be originated from anthropogenic sources, for example engines of vehicles (Vallero, 2014). In August 2017, the wildfire activities were so intense that the CO plumes raise from the fire region were much more significant than the background. This strong contrast makes CO a good tracer for the transport of the smoke plumes.

Figure 6 shows the evolution of the total column CO concentration (Texeira, 2013) every two days during the period of 11 August to 29 August 2017. CO concentration strongly increased in the west and north of Canada from 11 to 13 August, as

the UVAI in Figure 5. The forefront of the CO plume has reached the west and north of Europe since 19 August. We find that the spatial distribution and temporal evolution of CO are strongly co-related with the UVAI. This correlation is much evident before 21 August. After 21 August, the correlation became weaker, for the UVAI in North America was decreasing fast while the CO concentration remained almost unchanged or decreased much slower. It is possibly due to the longer lifetime of CO compared to UVAI. Combing the MODIS image, the UVAI and CO spatial-temporal evolution, we conclude that the aerosol plumes observed in Europe were smoke transported from Canada.

Reply To: AA **A12.**

3.6 CALIPSO measurements

CALIPSO measurements provide a good opportunity to investigate the vertical structure of the plumes and trace back the transport of the plumes. CALIPSO measures the backscattered signal at 532 and 1064 nm. One parallel channel and one perpendicular channel are coupled to derive particle linear depolarization ratio at 532 nm. Figure 7(a)–(f) present the profiles of the backscatter coefficient and particle linear depolarization ratio at 532 nm, corresponding to the six locations **a**–**f** in Figure 4. These data were obtained from the NASA Langley Research Center Atmospheric Science Data Center. The six locations are intendedly selected, falling in the region with elevated UVAI and CO concentration and following the transport pathway of the plume (in Figure 5 and 6) from Canada to Europe. Figure 7 shows the enhancements of backscatter in the upper troposphere and lower stratosphere. Aerosol and cloud are both possible causes of the backscatter enhancements and can be distinguished by using the particle depolarization ratio. We have examined the temperature profiles over several sites in North America in August 2017 and found that, above 10 km, the temperature drops below -38°C, at this temperature clouds consist mainly of ice crystals. The particle depolarization ratio is usually no less than 0.40 for ice cloud and from a few percent to about 0.40 for mixed-phase cloud.

Reply To: AA **A14.**

Figure 7(a) and (b) show the aerosol layers observed on 14 and 15 August over the north of Canada, both locations lay in the area where MODIS observed a smoke plume on 15 August (Figure 4) and the area with high UVAI and CO concentration. The particle linear depolarization ratio is about 0.05 in Figure 7(a) and 0.10 in (b), meaning that it is an aerosol layer instead of ice or mixed-phase cloud. Figure 7(c) and (f) show stratospheric layers detected at 10–20 km height, with the depolarization varying from 0.10 to 0.18. The lower layer at about 9 km in Figure 7(d) has depolarization ratio between 0.20 and 0.45 (median 0.32), which falls into the category of ice or mixed-phase clouds. Profiles in Figure 7(f) were captured over Berlin at 0129 UTC on 23 August. About 150 km in the south-west, a Lidar in Leipzig measured stratospheric smoke layers (Haarig et al., 2018). The particle depolarization ratio of CALIPSO at 532 nm on 23 August is consistent with ground based Lidar measurements in Lille and Leipzig, which will be presented in Section 4. It should be noted that aerosol types of the plumes in Figure 7 are quite uncertain in CALIPSO product. These layers are classified to scattered aerosol types, such as polluted dust, elevated smoke and volcanic ash. This mis-classification could introduce some extent of errors to the backscatter profile and particle depolarization

profiles.

Reply To: AR3 **A5.**, AA **A15.**

4 Results and analysis

4.1 Overview of retrieved optical parameters

We selected and averaged the Lidar measurement in 10 time intervals, among which five peroids are from LILAS system in Lille: 2200 (24 August) −0030 UTC (25 August), 1300 – 1600 UTC, 1600 – 1800 UTC (29 August), 2000 – 2300 (31 August) and 2300 (31 August)−0200 UTC (01 September); two intervals from IPRAL system in Palaiseau: 1600 – 1800 UTC and 1920 – 2120 UTC (28 August) and three intervals from the mobile Lidar in MAMS system (29 August): 1400 – 1500 UTC (corresponding spatially to 100 km distance from Palaiseau to Compiègne), 1500 – 1545 UTC (100 km on the route from Compiègne to Arras) and 1615 – 1630 UTC at Lille.

Figure 8 shows the optical depth of the stratospheric layer varying from 0.05 to 0.23 (at 532 nm). The spectral dependence of the optical depth of 355 nm and 532 nm is very weak. The maximal optical depth of the stratospheric layer was observed in the afternoon of 29 August, between 1600 and 1800 UTC. LILAS system observed aerosol optical depth of 0.20 ± 0.04 at 355 nm and 0.21 ± 0.04 at 532 nm. As discussed in Section 3.1, the columnar AOD at 532 nm from AERONET increased by about 0.20 after the presence of the stratospheric layer, which agrees well with the derived optical depth of the stratospheric layer. The minimum of the optical depth appeared in the night of 31 August 2017, giving 0.04 ± 0.02 at 355 nm and 0.05 ± 0.02 at 532 nm. The optical depth of the stratospheric layer along the route, observed by MAMS, are as follows: 0.19 over a distance of 100 km North from Palaiseau, 0.23 along 100 km of the middle of the transect from Compiègne to Arras and 0.22 when arriving at Lille.

Due to the insufficient signal-to-noise ratio above the stratospheric plume, the MAMS Lidar measurements are processed using Klett method, constraint by the columnar AOD measured by PLASMA sun photometer. Klett inversion is performed to the Lidar profile from the surface to the top of the stratospheric layer, assuming a vertically independent Lidar ratio. The optical depth of the stratospheric smoke layer is then calculated from the integral of the extinction profile. As a result, the error of the estimated smoke optical depth from MAMS measurements is difficult to quantify. Here we present the optical depth from MAMS Lidar for a comparison.

Reply To: AR1 **2.**

Table 2 summarizes the Lidar ratio and particle depolarization ratio in the stratospheric aerosol layer. Lidar ratios vary between 54 ± 9 sr and 58 ± 23 sr at 532 nm and between 31 ± 15 sr and 45 ± 9 sr at 355 nm. The results from two different Lidar systems and with different observation time agree well, indicating that the properties of the stratospheric layer are spatially and temporally stable. We derived higher Lidar ratio at 532 nm than at 355 nm which is a characteristic feature of aged smoke and

has been observed in previous studies (Wandinger et al., 2002; Murayama et al., 2004; Müller et al., 2005; Sugimoto et al., 2010). In the night of 31 August, the error of Lidar ratio is about $30-35\%$, relatively higher than the other days because of the low optical depth. Although the error varies, the mean values of derived Lidar ratio are relatively stable. The particle depolarization ratio decreases as wavelength increases. At 1064 nm channel, the particle linear depolarization ratio is very stable, varying from 0.040 ± 0.01 from 0.05 ± 0.01. At 532 nm channel, the depolarization is also stable, varying from 0.18 ± 0.03 to 0.20 ± 0.03. The particle linear depolarization ratio at 355 nm increased from 0.23 ± 0.03 on 24 August to 0.28 ± 0.08 on 31 August. However, the increase is within the range of the uncertainties. The particle depolarization ratio at 532 nm is in good agreement with CALIPSO observations shown in Figure 7(c)–(f). The particle depolarization ratio at 355 nm measured by LILAS is consistent with IPRAL system. (Haarig et al., 2018) measured 0.23 at 355 nm, 0.18 at 532 nm and 0.04 at 1064 nm in the stratospheric smoke layers on 22 August 2017, showing excellent agreements with our study.

The errors of particle depolarization ratio are calculated with the method in the Appendix. The estimated errors of the particle depolarization ratio are generally below 15%, expect the 355 nm channel in the night of 31 August when the optical depth was the lowest in all the investigated observations in this study. On 31 August, the backscatter ratio, volume depolarization ratio and molecular depolarization ratio at 355 nm are approximately: 3.5 (50%), 0.15 (10%) and 0.004 (200%). The values in the parentheses are the relative errors of the quantity on their left. The resulting error of particle depolarization is about 28%. At 532 nm channel, we derive 12% of error for the particle depolarization ratio when the backscatter ratio, volume depolarization ratio and molecular depolarization ratio are: 10 (50%), 0.15 (10%) and 0.004 (200%). In the same way, we derive less than 11% of error for the particle depolarization ratio at 1064 nm. The error at 355 nm is estimated to be higher than 532 and 1064 nm as the interferences of molecular scattering is stronger at this channel. When the layer is optically thicker, for example, 24 August, the error of 355 nm is estimated to be less than 13%. Conservatively, we use 30% for the error of particle linear depolarization ratio at 355 nm on 31 August and 15% for the error of the rest.

Reply To: AA **A19.** After re-calculation, we derived 0.28 ± 0.08 for the molecular depolarization ratio at 355 nm.

4.2 Case study

4.2.1 Optical properties

We select the night measurements of 24 August in Lille and 28 August in Palaiseau as two examples. The two systems were operating independently, so that the results from two different systems that measured at different time can be regarded as verifications for each other.

24 August 2017, Lille

Figure 9 shows the retrieved optical properties of the stratospheric smoke layer observed by LILAS system in the night of 24 August in Lille. The stratospheric aerosol layer is between 17 and 18 km, and we retrieved the extinction and backscatter profiles by assuming that the Lidar ratios are 36 sr at 355 nm and 54 sr at 532 nm. The Lidar ratio at 1064 nm channel is

assumed to be 60 sr. The extinction coefficient within the layer is about $0.12-0.22$ km^{-1} at 355 nm and 532 nm. It should be noted that the profile of the extinction coefficient is similar to the backscatter coefficient profile, because we assume the aerosol lidar ratio is vertically constant within the smoke layer. A comparison of backscatter coefficient profile has been made (not shown) between Klett and Raman method. We found that the difference of the backscatter coefficient profiles from the two methods are very consistent, indicating that our results are reliable. Assuming vertically constant aerosol Lidar ratio in the smoke layer is not unrealistic, as one can see that the particle linear depolarization ratios in the smoke layer have no noticeable vertical variation, indicating that the smoke particles are well mixed. The extinction-related Ångström exponent for 355 and 532 nm is around 0.0 ± 0.5, the backscatter-related Ångström exponent at corresponding wavelengths is about 1.0 ± 0.5. The particle depolarization ratios decrease as wavelength increases: 0.23±0.03 at 355 nm, 0.20±0.03 at 532 nm and 0.05±0.01 at 1064 nm. No parameters in Figure 9(b) exhibit noticeable vertical variations.

Reply To: AA **A17.**, AA **A22, 25.**

28 August 2017, Palaiseau

Figure 10 shows the retrieved optical parameters from IPRAL observations at $1920-2120$ UTC, 28 August 2017 in Palaiseau. The thickness of the stratospheric layer is about 2.3 km, spreading from 17.2 km to 19.5 km. Klett inversion was applied with estimated Lidar ratio of 36 sr at 355 nm and 58 sr at 532 nm. At 1064 nm the Lidar ratio was assumed to be 60 sr. The maximum extinction coefficient in the layer reached 0.12 km^{-1} at 532 nm. The extinction-related Ångström exponent between 355 nm and 532 nm is about -0.06±0.5. The corresponding backscatter Ångström exponent is about 1.2±0.5. The particle linear depolarization ratio at 355 nm is about 0.27±0.05. The particle linear depolarization ratio at 355 nm, extinction and backscatter-related Ångström exponent between 355 nm and 532 nm do not show evident vertical variations.

4.2.2 Microphysical properties

Regularization algorithm is applied to the vertically averaged extinction coefficients (at 355 and 532 nm) and backscatter coefficients (at 355, 532 and 1064 nm) in Figure 9 and Figure 10. Treating non-spherical particles is a challenging task. Many studies have been done to model the light scattering of non-spherical particles. The spheroid model was used to retrieved dust properties (Dubovik et al., 2006; Mishchenko et al., 1997; Veselovskii et al., 2010). But it is not clear if this model is applicable to soot particles with complicated morphology. The size of smoke particles is expected not too big so we choose to apply regularization algorithm with sphere model. The particle linear depolarization ratio is not used in the retrieval, and the spectral dependence of complex refractive indices is also ignored in the retrieval.The derived effective radius (R_{eff}), volume concentration (V_c), the real (m_R) and imaginary (m_I) part of the refractive indices are summarized in Table 3. The errors of the retrieved parameters have been discussed in the relevant papers (Müller et al., 1999; Veselovskii et al., 2002; Pérez-Ramírez et al., 2013). About 30% of relative error is derived for the reffective radius and volume concentration; $\pm$ 0.05 (absolute value) is expected for the real part of refractive indices and 50% is derived for the imaginary part of refractive radius.

Reply To: AR2 **A6.**

The retrieved particle size distributes in the range of 0.1 to 1.0 μm, with effective radius (volume-weighted sphere radius) of 0.33 ± 0.10 for both Palaiseau data and Lille data. The volume concentration is 15 ± 5 $\mu m^3 cm^{-3}$ for Palaiseau data and 22 ± 7 $\mu m^{-3} cm^3$ for Lille data. The real part of the complex refractive indices retrieved from Lille and Palaiseau data are also in good agreement, giving 1.55 ± 0.05 and 1.52 ± 0.05 for the real part, and 0.028 ± 0.014 and 0.021 ± 0.010 for the imaginary part. The single scattering albedos are estimated to be 0.82–0.89 for Lille data and 0.86–0.90 for Palaiseau data. The derived aerosol microphysical properties from Palaiseau and Lille data are consistent.

Reply To: AR3 **supplement.**

4.2.3 Direct radiative forcing effect

The stratospheric plumes observed on 24 and 28 August in Lille and Palaiseau are optically thick, with extinction coefficient about 10 times higher than in the volcanic ash observed by Ansmann et al. (1997) in April 1992, 10 months after the eruption of Mount Pinatubo. The radiative forcing imposed by the observed layers is a curious question. We input the retrieved microphysical properties into GARRLiC/GRASP to estimate the DRF effect of the stratospheric plumes in Lille and Palaiseau. We assume the vertical volume concentration of aerosols follows the extinction profile in Figure 9 and 10. The surface BRDF parameters for Lille and Palaiseau are taken from AERONET. The upward and downward flux/efficiencies, as well as the net DRF (ΔF, with respect to a pure Rayleigh atmosphere) of the stratospheric aerosol layers are calculated and Table 4 shows the daily averaged net DRF (W/m^2) at four levels: at the bottom of the atmosphere (BOA), below the stratospheric layer, above the stratospheric layer and at the top of the atmosphere (TOA). For the layer observed in Lille on 24 August, the top and base of the stratosphere are selected as: 18.4 km and 16.7 km and for Palaiseau observations, they are 20 km and 17.0 km.

At the top of the atmosphere, the net DRF flux is estimated to be -1.2 Wm^{-2} and -3.5 Wm^{-2} for Lille and Palaiseau data, respectively. The corresponding forcing efficiencies are -7.9 Wm$^{-2}\tau^{-1}$ and -21.5 Wm$^{-2}\tau^{-1}$. At the bottom of the atmosphere, the net DRF flux is estimated to -12.3 Wm^{-2} for Lille data and -14.5 Wm^{-2} for Palaiseau data. The corresponding forcing efficiencies are -79.6 Wm$^{-2}\tau^{-1}$ and -89.6 Wm$^{-2}\tau^{-1}$. We noticed that the difference in net DRF flux between the layer top and layer base is significant. For Lille data, we obtained 9.9 W/m^2 of difference between the top and the base of the stratospheric layer and for Palaiseau, we obtained 11.1 W/m^{-2}. Because of the high imaginary part of refractive indices, the stratospheric aerosols have the capacity of absorbing the incoming radiation, thus reducing the upward radiation at the top of the stratospheric layer and the downward radiation at the base of the stratospheric aerosol layer. The heating rate of the stratospheric layer is estimated to be 3.3 K/day for Palaiseau data and 3.7 K/day for Lille data. This qualitatively explains the increase of temperature within the stratospheric layer, as observed by the radiosonde measurements shown in Figure 3.

5 Discussion

The measurements revealed high particle depolarization ratios in the stratospheric smoke at 355 and 532 nm. In particular, the particle depolarization ratio at 355 nm is 0.23 ± 0.03 to 0.28 ± 0.08, while at 532 nm it is about 0.19 ± 0.03. The depolarization ratio at 1064 nm is significantly lower, about 0.05 ± 0.01. Similar spectral dependence of depolarization ratio3: 0.20, 0.09 and 0.02 at 355, 532 and 1064 nm, respectively, were observed by Burton et al. (2015) in a smoke plume at 7–8 km altitude (on 17 July 2014) in North American wildfires. Particle depolarization ratio of 0.07 and 0.02 at 532 and 1064 nm, respectively, were observed in a Canadian smoke plume at 6 km (on 02 August 2007) over the US (Burton et al., 2012). In Burton et al. (2012) and Burton et al. (2015), the smoke traveled approximately 3 days 6 days, respectively. The travel time in both cases are shorter than in our study. The light scattering process leading to high particle depolarization ratio of smoke particles is not well revealed yet. In previous studies, smoke mixed with soil particles was suggested to be the explanation (Fiebig et al., 2002; Murayama et al., 2004; Müller et al., 2007a; Sugimoto et al., 2010; Burton et al., 2012, 2015; Haarig et al., 2018). Strong convections occurred in fire activities, in principle are capable to lift soil particles into the smoke plume (Sugimoto et al., 2010). High depolarization ratio with similar spectral dependence has been observed in fine dust particles. Miffre et al. (2016) measured the particle depolarization ratio of two Arizona Test Dust samples at backscattering angle. The radii of the dust samples are mainly below 1 μm. They obtained higher depolarization ratio at 355 nm than at 532 nm, and the depolarization ratios at both wavelengths are over 0.30. The sharp edges and corners in the artificial dust samples are a possible reason for the measured high particle depolarization ratio. In the study of Järvinen et al. (2016), over 200 dust samples were used to measure the near-backscattering (178°) properties and it is found that, for fine-mode dust, the particle depolarization ratio has a strong size dependence. Järvinen et al. (2016) obtained about 0.12–0.20 and 0.25–0.30 for the depolarization ratio for equivalent particle size parameters at 355 and 532 nm in this study. Sakai et al. (2010) measured the depolarization of Asian and Saharan dust in the backscattering direction and obtained 0.14–0.17 at 532 nm for the samples with only sub-micrometer particles and 0.39 for the samples with high concentration of super-micrometer particles. Mamouri and Ansmann (2017) concluded that the depolarization spectrum of fine dust is: 0.21 $\pm$0.02 at 355 nm, 0.16 $\pm$0.02 at 532 nm and 0.09 $\pm$0.02 at 1064 nm. This spectrum is very similar to the Canadian stratospheric plume presented in this study and Haarig et al. (2018).

However, Murayama et al. (2004) suggested that the coagulation of smoke particles to the clusters with complicated morphology is a more reasonable explanation because they found no signature of mineral dust after analyzing the chemical compositions of the smoke samples. Mishchenko et al. (2016) modeled the spectral depolarization ratios observed by Burton et al. (2015) and found that such behavior is resulted from complicated morphology of smoke particles. Kahnert et al. (2012) modeled the optical properties of light absorbing carbon aggregates (LAC) embedded in a sulfate shell. It was found that the particle depolarization ratio increases with the aggregate radius (volume-equivalent sphere radius). For the case of 0.4 μm aggregate radius and 20% LAC volume fraction, the computed depolarization ratios are 0.12–0.20 at 304.0 nm, 0.08–0.18 at 533.1 nm and about 0.015 at 1010.1 nm, which are comparable with the results in this study and Haarig et al. (2018). In this study, we are not able to assess which is the dominant factor leading to the high depolarization ratios, possibly both soil particles and smoke aging process are partially responsible.

The derived Lidar ratios are from 31 ± 15 sr to 45 ± 9 sr for 355 nm and from 54 ± 12 sr to 58 ± 9 sr for 532 nm. Considering the uncertainties of the Lidar ratio, the derived values and the spectral dependence agree well with previous publications (Müller et al., 2005; Sugimoto et al., 2010; Haarig et al., 2018) about aged smoke observations. Haarig et al. (2018) obtained about 40 sr at 355 nm and 66 sr at 532 nm, using Raman method. The retrieved effective radius is about 0.33 ± 0.10 μm, consistent with the particle size obtained by Haarig et al. (2018). The particle size is larger than the values of fresh smoke observed near the fire source (O'Neill et al., 2002; Nicolae et al., 2013). In particular, the retrieved particle size agrees well with the observed smoke transported from Canada to Europe (Wandinger et al., 2002; Müller et al., 2005). Müller et al. (2007b) found that the effective radius increased from $0.15 - 0.25$ μm ($2 - 4$ days after the emission) to $0.3 - 0.4$ μm after $10 - 20$ days of transport time, which is consistent with our results. But it is worthy to be noted that Müller et al. (2007b) investigated only tropospheric smoke and it is not clear if this effect of aging process is applicable on stratospheric smoke.

Reply To: AA **A29.**

The real part of the refractive indices obtained in this study is 1.52±0.05 for Palaiseau data and 1.55±0.05 for Lille data, without considering the spectral dependence. The values are consistent with the results for tropospheric smoke (Dubovik et al., 2002; Wandinger et al., 2002; Taubman et al., 2004; Müller et al., 2005). As to the imaginary part, we derived 0.021 ± 0.010 from Palaiseau data and 0.028 ± 0.014 from Lille data. The imaginary part of refractive indices of smoke in previous studies is diverse. Müller et al. (2005) reported the imaginary part varying around 0.003 for non-absorbing tropospheric smoke originated from aged Siberian and Canadian forest fires. Wandinger et al. (2002) obtained $0.05 - 0.07$ for the imaginary part of Canadian smoke in the troposphere over Europe. Dubovik et al. (2002) derived about 0.01 to 0.03 for the imaginary part of biomass burning using photometer observations. The retrieved imaginary part in our study falls into the range of previously reported values. Using sphere model in the inversion is potentially an important error source, as spheres cannot fully represent the scattering of irregular aged smoke particles. The application on dust particles(Veselovskii et al., 2010) demonstrated that retrieved volume concentration and effective radius are still reliable and the main error is attributed to the imaginary part of refractive index. Errors in the optical data is also a potential source error of the retrieved microphysical parameters.

Reply To: AR1 **A3.** AR2 **A1.**

The relative humidity in the smoke layer is one factor that impacts the refractive indices, the particle depolarization ratio and Lidar ratio of smoke particles. While in some studies, the relative humidity is not mentioned, thus making the comparison difficult. Special attention should be paid to the relative humidity when comparing the complex refractive indices. Mixing with other aerosol types during transport is also a potential cause of the modification of aerosol properties, and its impact is not limited to the refractive indices. In this study, the smoke layers we observed were lofted to the lower stratosphere in the source region and then transported to the observation sites. They were isolated from other tropospheric aerosol sources and not likely to mix with them during the transport. The relative humidity in the stratospheric layer is below 10%, according to the radiosonde measurements. Our study provides a reference for aged smoke aerosols in a dry condition.

The retrieved particle parameters allow an estimation of direct aerosol radiative forcing. We derived -79.6 $Wm^{-2}\tau^{-1}$ and -7.9 $Wm^{-2}\tau^{-1}$ for the DRF efficiencies at the bottom and the top of the atmosphere for Lille data. And for Palaiseau data, we derived -89.6 $Wm^{-2}\tau^{-1}$ and -21.5 $Wm^{-2}\tau^{-1}$. It indicates that the observed stratospheric aerosol layers reduce strongly the radiation reaching the terrestrial surface mainly by absorbing solar radiation. Derimian et al. (2016) evaluated the radiative effect of several aerosol models, among which the daily net DRF efficiency of biomass burning aerosols is estimated to be -74 $Wm^{-2}\tau^{-1}$ to -54 $Wm^{-2}\tau^{-1}$ at the bottom of the atmosphere. Mallet et al. (2008) studied the radiative forcing of smoke and dust mixture over Djougou and derived -68 $Wm^{-2}\tau^{-1}$ to -50 $Wm^{-2}\tau^{-1}$ for the DRF efficiency at the bottom of the atmosphere. The uncertainties of the DRF estimation could be large, because of the high uncertainty in the retrieved microphysical properties, especially the imaginary part of the refractive indices. Our results show stronger forcing efficiencies, but are still comparable with the values in the publications. Additionally, the mean heating rate of the stratospheric smoke layer is estimated to be 3.7 K per day for Lille data and 3.3 K per day for Palaiseau data, which qualitatively supports the temperature increase within the stratospheric smoke layer. The warming effect in the layer is potentially responsible for the upward movements of soot-containing aerosol plumes (Laat et al., 2012; Ansmann et al., 2018).

Reply To: AR2 **A2.**

6 Conclusion

In the summer of 2017, large-scale wildfires spread in the west and north of Canada. The severe fire activities generated strong convections that lofted smoke plumes up to the high altitudes. After long-range transport, the smoke plumes spread over large areas. Three lidar systems in northern France observed aged smoke plumes in the stratosphere, about 10–17 days after intense fire emission. Unlike fresh smoke particles, the aged smoke particles showed surprisingly high particle depolarization ratios, indicating the presence of irregular smoke particles. Lidar data inversion revealed that the smoke particles are relatively bigger and very absorbing. The strong absorption of the observed smoke plumes is related to the perturbation of the temperature profile and the ascent of the plume when exposed to sunlight. In addition, the DRF estimation indicated that the stratospheric smoke can strongly reduce the radiation reaching the bottom of the atmosphere.

This study shows the capability of multi-wavelength Raman Lidar in aerosol profiling and characterization. We reported important optical and microphysical properties derived from Lidar observations, these results help to improve our knowledge about smoke particles and aerosol classification, which is an important topic in the Lidar community. Moreover, this event is also a good opportunity for the study of atmospheric model. The injection of smoke into upper troposphere and lower stratosphere by strong convection needs to be considered in atmospheric models. The self-lifting of absorbing smoke is not yet considered in any aerosol transport model. Additionally, this event provides a favorable chance for studying smoke aging process, the smoke plumes stayed more than one month in the stratosphere and were observed by ground-based Lidars and CALIPSO. However,

much more efforts are needed in investigating these measurements.

Reply To: AA **A31.**

Data availability. The satellite data from OMPS and AIRS can be found in NASA's GES DIS service center. CALIPSO data are obtained from the Langley Atmospheric Science Data Center. The radiosonde data are taken from the website of University of Wyoming (http://weather.uwyo.edu/upperair/sounding.html). All the lidar data used in this paper and data processing code or softwares are available upon request to the corresponding author.

Reply To: AR3 **supplement.**

Author contributions. QH carried the experiments in Lille station, processed the data and wrote the manuscript. PG supervised the project and did the manuscript correction. IV helped in the data analysis and manuscript correction. JBA contributed in providing IPRAL measurements and manuscript correction. IP performed experiments using MAMS system, analyzed the data and did manuscript corrections. TP contributed in LILAS measurements and calibration (with QH). MH and CP helped in manuscript correction and IPRAL operation. AL and XH contributed in developing and implementing GARRLiC/GRASP algorithm and radiative transfer code, respectively. CC helped in obtaining and interpreting satellite products. BT helped in manuscript correction.

Reply To: AR3 **supplement.**

Acknowledgements. We wish to thank ESA/IDEAS program (ESRIN/VEGA 4000111304/14/I-AM) who supported this work. FEDER/Region Hauts-de-France and CaPPA Labex are acknowledged for their support for LILAS multi-wavelength Raman LIDAR and MAMS system. H2020-ACTRIS-2/LiCAL Calibration center, EARLiNET, ACTRIS-France, ANRT France, CIMEL Electronique and Service National Observation PHOTONS/AERONET from CNRS-INSU are acknowledged for their support. The development of Lidar retrieval algorithms was supported by Russian Science Foundation (project 16-17-10241). The authors would like to acknowledge the use of GRASP inversion algorithm (http://www.grasp-open.com) in this work. NASA and the Langley Atmospheric Science Data Center are acknowledged for providing satellite products. The SIRTA observatory and supporting institutes are acknowledged for providing IPRAL data. Finally we thank all the co-authors for their kind cooperation and professional help.

Reply To: AR3 **supplement.**

Appendix A: Error estimation

A1 Errors of optical depth

The errors in the Lidar signal at the top and the base of the stratospheric layers are considered as the major error sources in the error estimation of the optical depth. We estimate the error of the Lidar signal $\overline{P}(\lambda, r_{top})$ and $\overline{P}(\lambda, r_{base})$ to be 3–5%, based on the statistical error of photon distributions. According to Equation 2, the error of the optical depth, $\frac{\Delta\tau^u}{\tau^u}$, is written as:

$$\left(\frac{\Delta\tau^u}{\tau^u}\right)^2 = F_{\overline{P}_{top}}\left(\frac{\Delta\overline{P}(\lambda, r_{top})}{\overline{P}(\lambda, r_{top})}\right)^2 + F_{\overline{P}_{base}}\left(\frac{\Delta\overline{P}(\lambda, r_{base})}{\overline{P}(\lambda, r_{base})}\right)^2 \tag{A1}$$

$$F_{\overline{P}_{top,base}} = \left(\frac{\overline{P}(\lambda, r_{top,base})}{\tau^u}\frac{\partial\tau^u}{\partial\overline{P}(\lambda, r_{top,base})}\right)^2 \tag{A2}$$

where $\Delta\tau^u$ represents the absolute error of τ^u. The calculation of molecular extinction and backscattering coefficient is based on the study of Bucholtz (1995). The temperature and pressure profiles are taken from the closest radiosonde stations, Trappes and Beauvechain, and the errors of molecular scattering are neglected.

Reply To: AR1 **1.** AR2 **A9.**

The error of optical depth propagates into Lidar ratio and vertically integrated backscatter coefficient. Additionally, the error of the Lidar ratio also relies on the step width of Lidar ratio between two consecutive iterations and the fitting error of the optical depth of the stratospheric aerosol layer, which can be limited by narrowing the step of the iteration. In our calculation, we use a step of 0.5 sr and achieve the fitting error of optical depth less than 1% which is negligible compared to the contribution of the error of optical depth to the error of Lidar ratio. However, we can basically estimate the error of the integral of the backscatter coefficient within the stratospheric aerosol layer, not the error of the backscatter coefficient profile.

A2 Errors of Ångström exponent

Ångström exponent $\mathring{A}$ is defined as follows:

$$\frac{x_{\lambda_1}}{x_{\lambda_2}} = (\frac{\lambda_1}{\lambda_2})^{-\mathring{A}} \tag{A3}$$

where x is usually the optical quantities such as optical depth τ, extinction coefficient α and backscatter coefficient β. The error of the Ångström exponent is resulted from the error of the optical quantities at two involved wavelengths:

$$(\Delta\mathring{A})^2 = \left(\log(\frac{\lambda_1}{\lambda_2})\right)^{-2}\left[(\frac{\Delta x_{\lambda_1}}{x_{\lambda_1}})^2 + (\frac{\Delta x_{\lambda_2}}{x_{\lambda_2}})^2\right] \tag{A4}$$

where Δx is the error of the quantity x in absolute values. In our study, when the error is 15% in the optical depth at 355 and 532 nm. The resulting error in the Ångström exponent is about 0.5.

A3 Errors of particle depolarization ratio

According to Equation 3, the error of particle depolarization ratio lies in three terms: the backscatter ratio R, volume depolarization δ_v ratio and molecular depolarization ratio δ_m.

$$\left(\frac{\Delta\delta_p}{\delta_p}\right)^2 = F_R\left(\frac{\Delta R}{R}\right)^2 + F_{\delta_v}\left(\frac{\Delta\delta_v}{\delta_v}\right)^2 + F_{\delta_m}\left(\frac{\Delta\delta_m}{\delta_m}\right)^2 \tag{A5}$$

$$F_X = \left(\frac{X}{\delta_p}\frac{\partial\delta_p}{\partial X}\right)^2, X = R,\ \delta_v,\ \delta_m \tag{A6}$$

As the backscatter ratio and the volume depolarization increase, the dependence of particle depolarization ratio on the backscatter ratio decreases. In the stratospheric smoke layer, the measured volume depolarization ratio is higher in the shorter wavelength and the backscatter ratio is higher in the longer wavelength, the increased volume depolarization ratio or the backscatter ratio allow us to conservatively assume a preliminary error level for the backscatter ratio R. The potential error sources of the volume depolarization come from the optics and the polarization calibration. The optics have been carefully maintained and adjusted to minimize the errors originated from misalignments. After long-term Lidar operation and monitoring of the depolarization calibration, we conservatively expect 10% relative errors in the volume depolarization ratio. The theoretical molecular depolarization ratio is calculated to be 0.0036 with negligible wavelength dependence (Miles et al., 2001; She, 2001). In the historical record since 2013, LILAS measured molecular depolarization ratios ofapproximately 0.008–0.013 at 532 nm channel, 0.012–0.018 at 355 nm channel and 0.007–0.010 at 1064 nm channel. IPRAL measured molecular depolarization ratio about 0.020 at 355 nm in this study. Molecular depolarization ratios measured by both LILAS and IPRAL system exceed the theoretical value. In addition to the error in the polarization calibration, the error of molecular depolarization ratio rises mainly from the optics, precisely, the cross-talks between the two polarization channels. The imperfections of the optics cannot be avoided, but a careful characterization is helpful to eliminate the cross-talks as much as possible (Freudenthaler, 2016). In our study, we simply assume 200% and 300% for the error of molecular depolarization ratio measured by LILAS and IPRAL system, respectively. The total error of particle depolarization ratio is calculated according to Equation A5.

References

Andreae, M. O., Browell, E. V., Garstang, M., Gregory, G., Harriss, R., Hill, G., Jacob, D. J., Pereira, M., Sachse, G., Setzer, A., et al.: Biomass-burning emissions and associated haze layers over Amazonia, Journal of Geophysical Research: Atmospheres, 93, 1509–1527, 1988.

Ansmann, A., Riebesell, M., Wandinger, U., Weitkamp, C., Voss, E., Lahmann, W., and Michaelis, W.: Combined Raman elastic-backscatter lidar for vertical profiling of moisture, aerosol extinction, backscatter, and lidar ratio, Applied Physics B: Lasers and Optics, 55, 18–28, 1992.

Ansmann, A., Mattis, I., Wandinger, U., Wagner, F., Reichardt, J., and Deshler, T.: Evolution of the Pinatubo aerosol: Raman lidar observations of particle optical depth, effective radius, mass, and surface area over Central Europe at 53.4 N, Journal of the atmospheric sciences, 54, 2630–2641, 1997.

Ansmann, A., Baars, H., Chudnovsky, A., Mattis, I., Veselovskii, I., Haarig, M., Seifert, P., Engelmann, R., and Wandinger, U.: Extreme levels of Canadian wildfire smoke in the stratosphere over central Europe on 21–22 August 2017, Atmospheric Chemistry and Physics, 18, 11 831–11 845, 2018.

Böckmann, C., Wandinger, U., Ansmann, A., Bösenberg, J., Amiridis, V., Boselli, A., Delaval, A., De Tomasi, F., Frioud, M., Grigorov, I. V., et al.: Aerosol lidar intercomparison in the framework of the EARLINET project. 2. Aerosol backscatter algorithms, Applied Optics, 43, 977–989, 2004.

Bösenberg, J., Matthias, V., Linné, H., Comerón Tejero, A., Rocadenbosch Burillo, F., Pérez López, C., and Baldasano Recio, J. M.: EARLINET: A European Aerosol Research Lidar Network to establish an aerosol climatology, Report. Max-Planck-Institut fur Meteorologie, pp. 1–191, 2003.

Bovchaliuk, V., Goloub, P., Podvin, T., Veselovskii, I., Tanre, D., Chaikovsky, A., Dubovik, O., Mortier, A., Lopatin, A., Korenskiy, M., et al.: Comparison of aerosol properties retrieved using GARRLiC, LIRIC, and Raman algorithms applied to multi-wavelength lidar and sun/sky-photometer data, Atmospheric Measurement Techniques, 9, 3391–3405, 2016.

Bravo-Aranda, J. A., Belegante, L., Freudenthaler, V., Alados-Arboledas, L., Nicolae, D., Granados-Muñoz, M. J., Guerrero-Rascado, J. L., Amodeo, A., D'Amico, G., Engelmann, R., et al.: Assessment of lidar depolarization uncertainty by means of a polarimetric lidar simulator, Atmospheric Measurement Techniques, 9, 4935, 2016.

Bucholtz, A.: Rayleigh-scattering calculations for the terrestrial atmosphere, Applied Optics, 34, 2765–2773, 1995.

Burton, S., Ferrare, R., Hostetler, C., Hair, J., Rogers, R., Obland, M., Butler, C., Cook, A., Harper, D., and Froyd, K.: Aerosol classification using airborne High Spectral Resolution Lidar measurements-methodology and examples, Atmospheric Measurement Techniques, 5, 73, 2012.

Burton, S., Hair, J., Kahnert, M., Ferrare, R., Hostetler, C., Cook, A., Harper, D., Berkoff, T., Seaman, S., Collins, J., et al.: Observations of the spectral dependence of linear particle depolarization ratio of aerosols using NASA Langley airborne High Spectral Resolution Lidar, Atmospheric Chemistry and Physics, 15, 13 453–13 473, 2015.

Derimian, Y., Dubovik, O., Huang, X., Lapyonok, T., Litvinov, P., Kostinski, A. B., Dubuisson, P., and Ducos, F.: Comprehensive tool for calculation of radiative fluxes: illustration of shortwave aerosol radiative effect sensitivities to the details in aerosol and underlying surface characteristics, Atmospheric Chemistry and Physics, 16, 5763–5780, 2016.

Deshler, T.: A review of global stratospheric aerosol: Measurements, importance, life cycle, and local stratospheric aerosol, Atmospheric Research, 90, 223–232, 2008.

Dubovik, O., Holben, B., Eck, T. F., Smirnov, A., Kaufman, Y. J., King, M. D., Tanré, D., and Slutsker, I.: Variability of absorption and optical properties of key aerosol types observed in worldwide locations, Journal of the atmospheric sciences, 59, 590–608, 2002.

Dubovik, O., Sinyuk, A., Lapyonok, T., Holben, B. N., Mishchenko, M., Yang, P., Eck, T. F., Volten, H., Munoz, O., Veihelmann, B., et al.: Application of spheroid models to account for aerosol particle nonsphericity in remote sensing of desert dust, Journal of Geophysical Research: Atmospheres, 111, 2006.

Dubovik, O., Lapyonok, T., Litvinov, P., Herman, M., Fuertes, D., Ducos, F., Lopatin, A., Chaikovsky, A., Torres, B., Derimian, Y., et al.: GRASP: a versatile algorithm for characterizing the atmosphere, SPIE Newsroom, 25, 2014.

Fiebig, M., Petzold, A., Wandinger, U., Wendisch, M., Kiemle, C., Stifter, A., Ebert, M., Rother, T., and Leiterer, U.: Optical closure for an aerosol column: Method, accuracy, and inferable properties applied to a biomass-burning aerosol and its radiative forcing, Journal of Geophysical Research: Atmospheres, 107, 2002.

Freudenthaler, V.: About the effects of polarising optics on lidar signals and the Delta 90 calibration, Atmospheric Measurement Techniques, pp. 4181–4255, 2016.

Freudenthaler, V., Esselborn, M., Wiegner, M., Heese, B., Tesche, M., Ansmann, A., Müller, D., Althausen, D., Wirth, M., Fix, A., et al.: Depolarization ratio profiling at several wavelengths in pure Saharan dust during SAMUM 2006, Tellus B, 61, 165–179, 2009.

Freudenthaler, V., Linné, H., Chaikovski, A., Rabus, D., and Groß, S.: EARLINET lidar quality assurance tools, 2018.

Fromm, M., Alfred, J., Hoppel, K., Hornstein, J., Bevilacqua, R., Shettle, E., Servranckx, R., Li, Z., and Stocks, B.: Observations of boreal forest fire smoke in the stratosphere by POAM III, SAGE II, and lidar in 1998, Geophysical Research Letters, 27, 1407–1410, 2000.

Fromm, M., Bevilacqua, R., Servranckx, R., Rosen, J., Thayer, J. P., Herman, J., and Larko, D.: Pyro-cumulonimbus injection of smoke to the stratosphere: Observations and impact of a super blowup in northwestern Canada on 3–4 August 1998, Journal of Geophysical Research: Atmospheres, 110, 2005.

Fromm, M., Shettle, E., Fricke, K., Ritter, C., Trickl, T., Giehl, H., Gerding, M., Barnes, J., O'Neill, M., Massie, S., et al.: Stratospheric impact of the Chisholm pyrocumulonimbus eruption: 2. Vertical profile perspective, Journal of Geophysical Research: Atmospheres, 113, 2008.

Fromm, M. D. and Servranckx, R.: Transport of forest fire smoke above the tropopause by supercell convection, Geophysical Research Letters, 30, 2003.

Haarig, M., Ansmann, A., Baars, H., Jimenez, C., Veselovskii, I., Engelmann, R., and Althausen, D.: Depolarization and lidar ratios at 355, 532, and 1064 nm and microphysical properties of aged tropospheric and stratospheric Canadian wildfire smoke, Atmospheric Chemistry and Physics, 18, 11 847–11 861, 2018.

Haeffelin, M., Barthès, L., Bock, O., Boitel, C., Bony, S., Bouniol, D., Chepfer, H., Chiriaco, M., Cuesta, J., Delanoë, J., et al.: SIRTA, a ground-based atmospheric observatory for cloud and aerosol research, in: Annales Geophysicae, vol. 23, pp. 253–275, 2005.

Haskins, R. and Kaplan, L.: Remote sensing of trace gases using the Atmospheric InfraRed Sounder, in: IRS, vol. 92, pp. 278–281, 1992.

Hofmann, D., Barnes, J., O'Neill, M., Trudeau, M., and Neely, R.: Increase in background stratospheric aerosol observed with lidar at Mauna Loa Observatory and Boulder, Colorado, Geophysical Research Letters, 36, 2009.

Hsu, N. C., Herman, J., Torres, O., Holben, B., Tanre, D., Eck, T., Smirnov, A., Chatenet, B., and Lavenu, F.: Comparisons of the TOMS aerosol index with Sun-photometer aerosol optical thickness: Results and applications, Journal of Geophysical Research: Atmospheres, 104, 6269–6279, 1999.

Jaross, G.: OMPS-NPP L3 NM Ozone (O3) Total Column 1.0 deg grid daily V2, Greenbelt, MD, USA, Goddard Earth Sciences Data and Information Services Center (GES DISC), https://doi.org/10.5067/7Y7KSA1QNQP8, accessed: 2018-04-28, 2017.

Järvinen, E., Kemppinen, O., Nousiainen, T., Kociok, T., Möhler, O., Leisner, T., and Schnaiter, M.: Laboratory investigations of mineral dust near-backscattering depolarization ratios, Journal of Quantitative Spectroscopy and Radiative Transfer, 178, 192–208, 2016.

Kahn, B., Irion, F., Dang, V., Manning, E., Nasiri, S., Naud, C., Blaisdell, J., Schreier, M., Yue, Q., Bowman, K., et al.: The atmospheric infrared sounder version 6 cloud products, Atmospheric Chemistry and Physics, 14, 399, 2014.

Kahnert, M., Nousiainen, T., Lindqvist, H., and Ebert, M.: Optical properties of light absorbing carbon aggregates mixed with sulfate: assessment of different model geometries for climate forcing calculations, Optics express, 20, 10 042–10 058, 2012.

Karol, Y., Tanré, D., Goloub, P., Vervaerde, C., Balois, J., Blarel, L., Podvin, T., Mortier, A., and Chaikovsky, A.: Airborne sun photometer PLASMA: concept, measurements, comparison of aerosol extinction vertical profile with lidar, Atmospheric Measurement Techniques, 6, 2383, 2013.

Khaykin, S., Godin-Beekmann, S., Hauchecorne, A., Pelon, J., Ravetta, F., and Keckhut, P.: Stratospheric smoke with unprecedentedly high backscatter observed by lidars above southern France, Geophysical Research Letters, 45, 1639–1646, 2018.

Khaykin, S. M., Godin-Beekmann, S., Keckhut, P., Hauchecorne, A., Jumelet, J., Vernier, J.-P., Bourassa, A., Degenstein, D. A., Rieger, L. A., Bingen, C., et al.: Variability and evolution of the midlatitude stratospheric aerosol budget from 22 years of ground-based lidar and satellite observations, Atmospheric Chemistry and Physics, 17, 1829–1845, 2017.

Klett, J. D.: Lidar inversion with variable backscatter/extinction ratios, Applied Optics, 24, 1638–1643, 1985.

Kremser, S., Thomason, L. W., Hobe, M., Hermann, M., Deshler, T., Timmreck, C., Toohey, M., Stenke, A., Schwarz, J. P., Weigel, R., et al.: Stratospheric aerosol?Observations, processes, and impact on climate, Reviews of Geophysics, 54, 278–335, 2016.

Laat, A., Stein Zweers, D. C., and Boers, R.: A solar escalator: Observational evidence of the self-lifting of smoke and aerosols by absorption of solar radiation in the February 2009 Australian Black Saturday plume, Journal of Geophysical Research: Atmospheres, 117, 2012.

Lenoble, J., Herman, M., Deuzé, J., Lafrance, B., Santer, R., and Tanré, D.: A successive order of scattering code for solving the vector equation of transfer in the earth's atmosphere with aerosols, Journal of Quantitative Spectroscopy and Radiative Transfer, 107, 479–507, 2007.

Lopatin, A., Dubovik, O., Chaikovsky, A., Goloub, P., Lapyonok, T., Tanré, D., and Litvinov, P.: Enhancement of aerosol characterization using synergy of lidar and sun-photometer coincident observations: the GARRLiC algorithm, Atmospheric Measurement Techniques, 6, 2065, 2013.

Luderer, G., Trentmann, J., Winterrath, T., Textor, C., Herzog, M., Graf, H., and Andreae, M.: Modeling of biomass smoke injection into the lower stratosphere by a large forest fire (Part II): sensitivity studies, Atmospheric Chemistry and Physics, 6, 5261–5277, 2006.

Mallet, M., Pont, V., Liousse, C., Gomes, L., Pelon, J., Osborne, S., Haywood, J., Roger, J.-C., Dubuisson, P., Mariscal, A., et al.: Aerosol direct radiative forcing over Djougou (northern Benin) during the African Monsoon Multidisciplinary Analysis dry season experiment (Special Observation Period-0), Journal of Geophysical Research: Atmospheres, 113, 2008.

Mamouri, R. and Ansmann, A.: Potential of polarization/Raman lidar to separate fine dust, coarse dust, maritime, and anthropogenic aerosol profiles, Atmos, Meas. Tech, 10, 3403–3427, 2017.

Matthais, V., Freudenthaler, V., Amodeo, A., Balin, I., Balis, D., Bösenberg, J., Chaikovsky, A., Chourdakis, G., Comeron, A., Delaval, A., et al.: Aerosol lidar intercomparison in the framework of the EARLINET project. 1. Instruments, Applied Optics, 43, 961–976, 2004.

McMillan, W., Barnet, C., Strow, L., Chahine, M., McCourt, M., Warner, J., Novelli, P., Korontzi, S., Maddy, E., and Datta, S.: Daily global maps of carbon monoxide from NASA's Atmospheric Infrared Sounder, Geophysical Research Letters, 32, 2005.

McPeters, R. D., Bhartia, P., Krueger, A. J., Herman, J. R., Wellemeyer, C. G., Seftor, C. J., Byerly, W., and Celarier, E. A.: Total Ozone Mapping Spectrometer (TOMS) Level-3 data products user's guide, 2000.

Miffre, A., Mehri, T., Francis, M., and Rairoux, P.: UV–VIS depolarization from Arizona Test Dust particles at exact backscattering angle, Journal of Quantitative Spectroscopy and Radiative Transfer, 169, 79–90, 2016.

Miles, R. B., Lempert, W. R., and Forkey, J. N.: Laser rayleigh scattering, Measurement Science and Technology, 12, R33, 2001.

Mishchenko, M. I., Travis, L. D., Kahn, R. A., and West, R. A.: Modeling phase functions for dustlike tropospheric aerosols using a shape mixture of randomly oriented polydisperse spheroids, Journal of Geophysical Research: Atmospheres, 102, 16 831–16 847, 1997.

Mishchenko, M. I., Dlugach, J. M., and Liu, L.: Linear depolarization of lidar returns by aged smoke particles, Applied optics, 55, 9968–9973, 2016.

Müller, D., Wandinger, U., and Ansmann, A.: Microphysical particle parameters from extinction and backscatter lidar data by inversion with regularization: theory, Applied Optics, 38, 2346–2357, 1999.

Müller, D., Mattis, I., Wandinger, U., Ansmann, A., Althausen, D., and Stohl, A.: Raman lidar observations of aged Siberian and Canadian forest fire smoke in the free troposphere over Germany in 2003: Microphysical particle characterization, Journal of Geophysical Research: Atmospheres, 110, 2005.

Müller, D., Ansmann, A., Mattis, I., Tesche, M., Wandinger, U., Althausen, D., and Pisani, G.: Aerosol-type-dependent lidar ratios observed with Raman lidar, Journal of Geophysical Research: Atmospheres, 112, 2007a.

Müller, D., Mattis, I., Ansmann, A., Wandinger, U., Ritter, C., and Kaiser, D.: Multiwavelength Raman lidar observations of particle growth during long-range transport of forest-fire smoke in the free troposphere, Geophysical Research Letters, 34, 2007b.

Murayama, T., Müller, D., Wada, K., Shimizu, A., Sekiguchi, M., and Tsukamoto, T.: Characterization of Asian dust and Siberian smoke with multi-wavelength Raman lidar over Tokyo, Japan in spring 2003, Geophysical Research Letters, 31, 2004.

Nicolae, D., Nemuc, A., Müller, D., Talianu, C., Vasilescu, J., Belegante, L., and Kolgotin, A.: Characterization of fresh and aged biomass burning events using multiwavelength Raman lidar and mass spectrometry, Journal of Geophysical Research: Atmospheres, 118, 2956–2965, 2013.

O'Neill, N., Eck, T., Holben, B., Smirnov, A., Royer, A., and Li, Z.: Optical properties of boreal forest fire smoke derived from Sun photometry, Journal of Geophysical Research: Atmospheres, 107, 2002.

Papayannis, A., Amiridis, V., Mona, L., Tsaknakis, G., Balis, D., Bösenberg, J., Chaikovski, A., De Tomasi, F., Grigorov, I., Mattis, I., et al.: Systematic lidar observations of Saharan dust over Europe in the frame of EARLINET (2000–2002), Journal of Geophysical Research: Atmospheres, 113, 2008.

Pappalardo, G., Amodeo, A., Apituley, A., Comeron, A., Freudenthaler, V., Linné, H., Ansmann, A., Bösenberg, J., D'Amico, G., Mattis, I., et al.: EARLINET: towards an advanced sustainable European aerosol lidar network, Atmospheric Measurement Techniques, pp. 2389–2409, 2014.

Pérez-Ramírez, D., Whiteman, D., Veselovskii, I., Kolgotin, A., Korenskiy, M., and Alados-Arboledas, L.: Effects of systematic and random errors on the retrieval of particle microphysical properties from multiwavelength lidar measurements using inversion with regularization, Atmospheric Measurement Techniques, 6, 3039–3054, 2013.

Platt, C.: Lidar and radiometric observations of cirrus clouds, Journal of the atmospheric sciences, 30, 1191–1204, 1973.

Popovici, I. E., Goloub, P., Podvin, T., Blarel, L., Loisil, R., Unga, F., Mortier, A., Deroo, C., Victori, S., Ducos, F., et al.: Description and applications of a mobile system performing on-road aerosol remote sensing and in situ measurements, Atmospheric Measurement Techniques Discussions, 2018.

Sakai, T., Nagai, T., Zaizen, Y., and Mano, Y.: Backscattering linear depolarization ratio measurements of mineral, sea-salt, and ammonium sulfate particles simulated in a laboratory chamber, Applied optics, 49, 4441–4449, 2010.

Sassen, K., Liou, K. N., Kinne, S., and Griffin, M.: Highly supercooled cirrus cloud water: Confirmation and climatic implications, Science, 227, 411–413, 1985.

Seftor, C., Jaross, G., Kowitt, M., Haken, M., Li, J., and Flynn, L.: Postlaunch performance of the Suomi National Polar-orbiting Partnership Ozone Mapping and Profiler Suite (OMPS) nadir sensors, Journal of Geophysical Research: Atmospheres, 119, 4413–4428, 2014.

She, C.-Y.: Spectral structure of laser light scattering revisited: bandwidths of nonresonant scattering lidars, Applied optics, 40, 4875–4884, 2001.

Shepherd, T. G.: Transport in the middle atmosphere, Journal of the Meteorological Society of Japan. Ser. II, 85, 165–191, 2007.

Sugimoto, N., Tatarov, B., Shimizu, A., Matsui, I., and Nishizawa, T.: Optical characteristics of forest-fire smoke observed with two-wavelength Mie-scattering lidars and a high-spectral-resolution lidar over Japan, SOLA, 6, 93–96, 2010.

Susskind, J., Blaisdell, J. M., and Iredell, L.: Improved methodology for surface and atmospheric soundings, error estimates, and quality control procedures: the atmospheric infrared sounder science team version-6 retrieval algorithm, Journal of Applied Remote Sensing, 8, 084 994, 2014.

Taubman, B. F., Marufu, L. T., Vant-Hull, B. L., Piety, C. A., Doddridge, B. G., Dickerson, R. R., and Li, Z.: Smoke over haze: Aircraft observations of chemical and optical properties and the effects on heating rates and stability, Journal of Geophysical Research: Atmospheres, 109, 2004.

Texeira, A. S. T.: AIRS/Aqua L3 Daily Standard Physical Retrieval (AIRS-only) 1 degree x 1 degree V006, Greenbelt, MD, USA, Goddard Earth Sciences Data and Information Services Center (GES DISC), https://doi.org/10.5067/Aqua/AIRS/DATA303, accessed: 2018-04-28, 2013.

Trentmann, J., Luderer, G., Winterrath, T., Fromm, M., Servranckx, R., Textor, C., Herzog, M., Graf, H.-F., and Andreae, M.: Modeling of biomass smoke injection into the lower stratosphere by a large forest fire (Part I): reference simulation, Atmospheric Chemistry and Physics, 6, 5247–5260, 2006.

Vallero, D.: Fundamentals of air pollution, Academic press, 2014.

Veselovskii, I., Kolgotin, A., Griaznov, V., Müller, D., Wandinger, U., and Whiteman, D. N.: Inversion with regularization for the retrieval of tropospheric aerosol parameters from multiwavelength lidar sounding, Applied optics, 41, 3685–3699, 2002.

Veselovskii, I., Dubovik, O., Kolgotin, A., Lapyonok, T., Di Girolamo, P., Summa, D., Whiteman, D. N., Mishchenko, M., and Tanré, D.: Application of randomly oriented spheroids for retrieval of dust particle parameters from multiwavelength lidar measurements, Journal of Geophysical Research: Atmospheres, 115, 2010.

Veselovskii, I., Goloub, P., Podvin, T., Bovchaliuk, V., Derimian, Y., Augustin, P., Fourmentin, M., Tanre, D., Korenskiy, M., Whiteman, D., et al.: Retrieval of optical and physical properties of African dust from multiwavelength Raman lidar measurements during the SHADOW campaign in Senegal, Atmos. Chem. Phys, 16, 7013–7028, 2016.

Veselovskii, I., Goloub, P., Podvin, T., Tanre, D., Ansmann, A., Korenskiy, M., Borovoi, A., Hu, Q., and Whiteman, D.: Spectral dependence of backscattering coefficient of mixed phase clouds over West Africa measured with two-wavelength Raman polarization lidar: Features attributed to ice-crystals corner reflection, Journal of Quantitative Spectroscopy and Radiative Transfer, 202, 74–80, 2017.

Wandinger, U., Müller, D., Böckmann, C., Althausen, D., Matthias, V., Bösenberg, J., Weiß, V., Fiebig, M., Wendisch, M., Stohl, A., et al.: Optical and microphysical characterization of biomass-burning and industrial-pollution aerosols from-multiwavelength lidar and aircraft measurements, Journal of Geophysical Research: Atmospheres, 107, 2002.

Young, S. A.: Analysis of lidar backscatter profiles in optically thin clouds, Applied optics, 34, 7019–7031, 1995.

Zuev, V. V., Burlakov, V. D., Nevzorov, A. V., Pravdin, V. L., Savelieva, E. S., and Gerasimov, V. V.: 30-year lidar observations of the stratospheric aerosol layer state over Tomsk (Western Siberia, Russia), Atmospheric Chemistry and Physics, 17, 3067–3081, 2017.

Table 1. Three involved lidar systems, their configuration and locations.

Name	Configuration	Location
LILAS	Elastic + depolarizatiom: 355, 532, 1064 nm Raman: 387, 408 (water vapor), 530 nm	LOA, Lille
IPRAL	Elastic: 355 (depolarization), 532, 1064 nm Raman: 387, 408 (water vapor), 608 nm	SIRTA, Palaiseau
MAMS Lidar	Elastic: 532 nm	from Palaiseau to Lille (29 August)

Reply To: AR3 **supplement.**

5

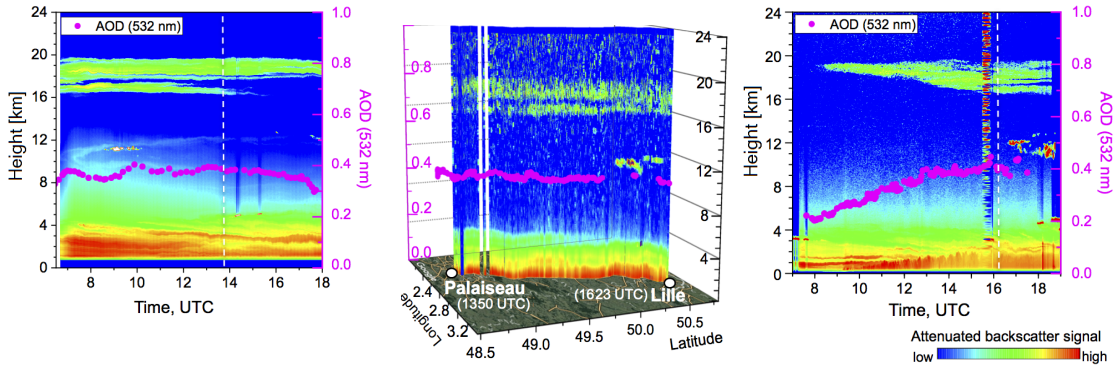

(a) (b) (c)

Figure 1. Lidar range-corrected signal and columnar AOD from sun photometer at 532 nm, 29 August 2017. (a) IPRAL system in Palaiseau. (b) MAMS Lidar on-route from Palaiseau to Lille. (c) LILAS in Lille. Columnar AOD measurements are interpolated from AERONET (Lille and Palaiseau) and PLASMA (mobile system) measurements. MAMS started from Palaiseau at 1353 UTC and arrived in Lille at 1623 UTC. The departure and arriving time are indicated in (a) and (c) with the white dashed lines.

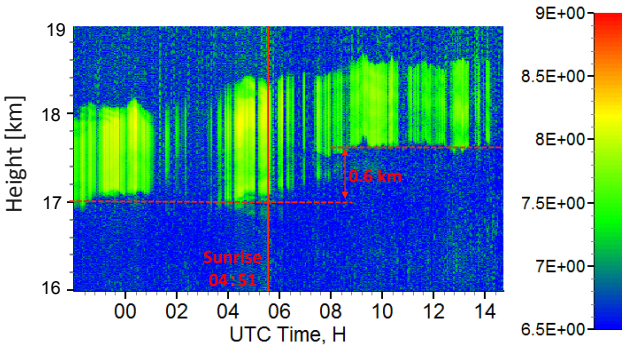

Figure 2. Lidar range-corrected signal at 1064 nm on 24–25 August 2017 measured by LILAS. The red solid line indicates the sunrise time. The two red dashed lines point out the approximate layer base before and after the sunrise. The sunrise and sunset time are 04:51 UTC and 20:47 UTC, respectively. The corresponding daytime duration is about 14 hours.

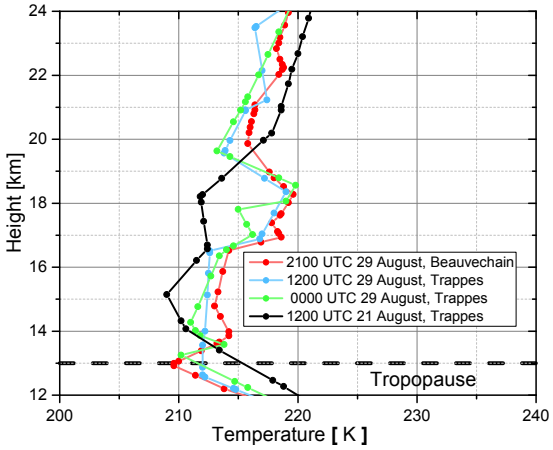

Figure 3. Temperature profiles from the radiosonde measurements. The green and cerulean lines are the temperature profiles of Trappes at 0000 and 1200 UTC, 29 August 2017. The red line shows the Beauvechain data at 2100 UTC 29 August 2017. The black line is for 1200 UTC, 21 August, Trappes. The horizontal black dashed line at 13 km represents the approximate position of the tropopause.

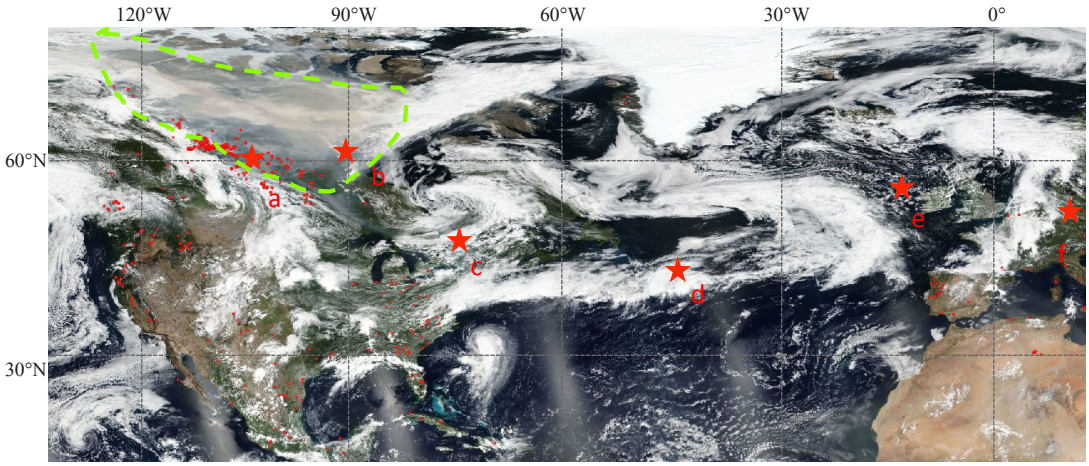

Figure 4. The corrected surface reflectance overlaid with fire and thermal anomalies from MODIS (15 August 2017). The region marked with green dashed line in the northwest indicated a plume generated by fire activities. Six locations (labeled as red stars) on the tracks of CALIPSO are selected: **a** (61.47°N, 106.44°W), **b** (62.79°N, 91.54°W), **c** (46.97°N, 72.22°W), **d** (42.27°N, 42.08°W), **e** (55.97°N, 12.54°W) and **f** (52.37°N, 13.47°E). The corresponding overpass date is 14, 15, 17, 19, 21 and 23 August 2017.

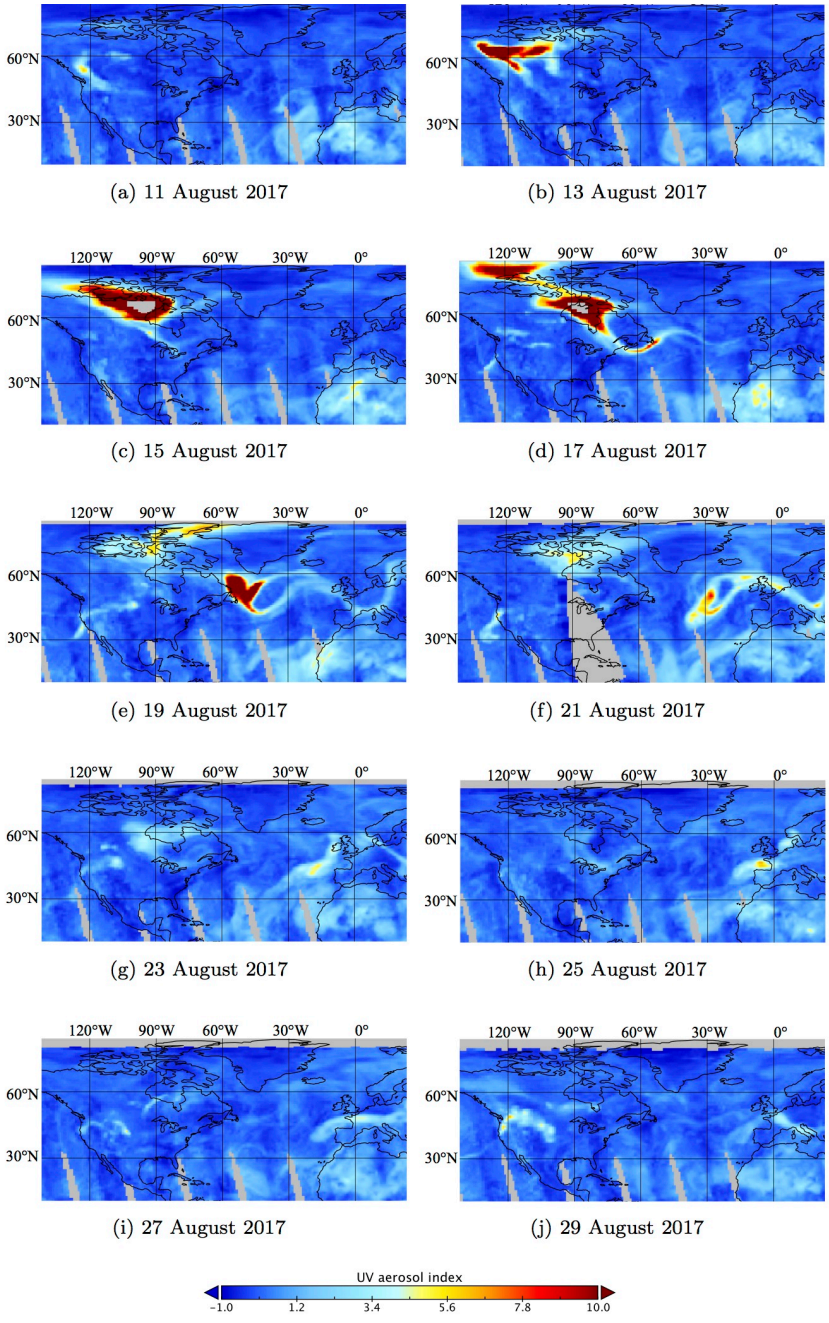

Figure 5. OMPS NM daily UVAI products during 11 to 29 August 2017. The results are plotted every two days. Grey colour indicates areas with no retrievals.

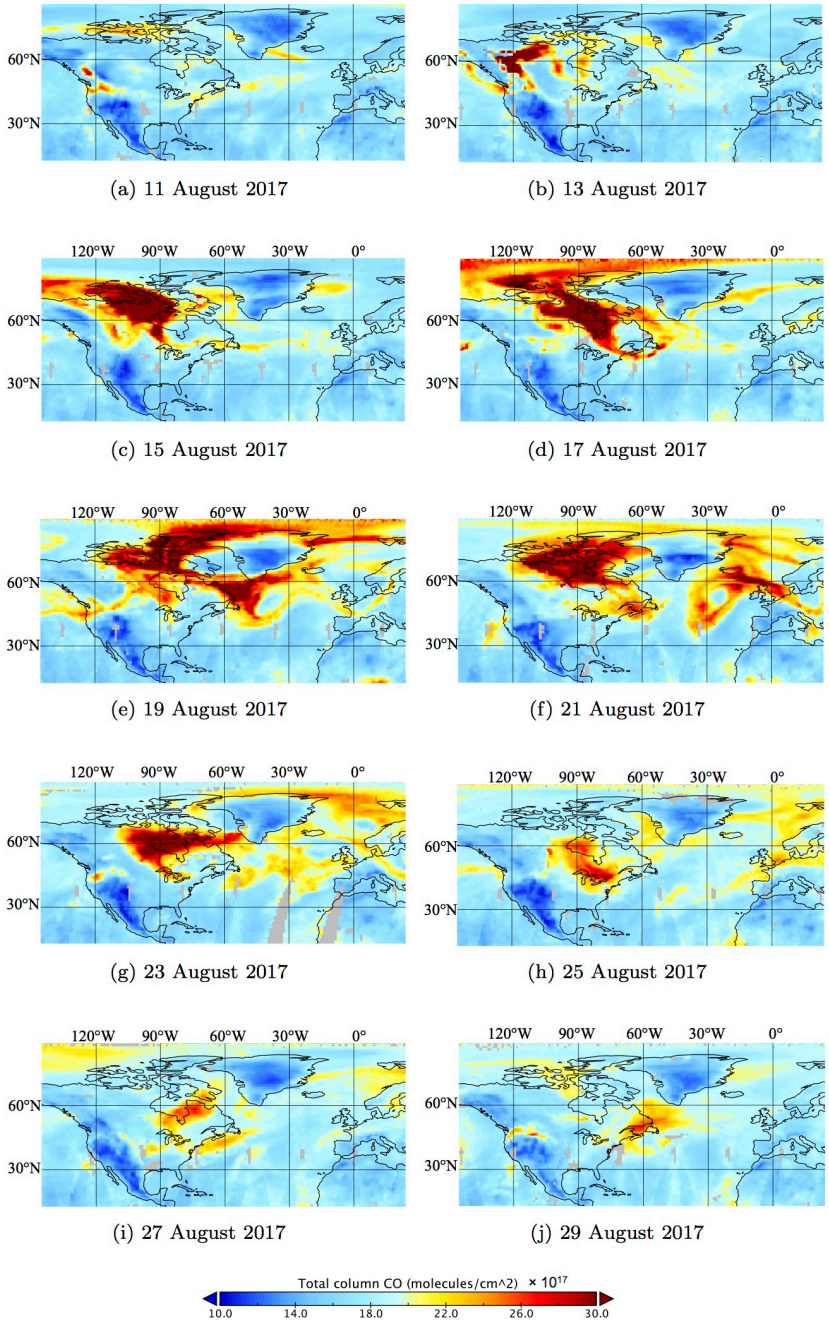

(a) 11 August 2017 (b) 13 August 2017

(c) 15 August 2017 (d) 17 August 2017

(e) 19 August 2017 (f) 21 August 2017

(g) 23 August 2017 (h) 25 August 2017

(i) 27 August 2017 (j) 29 August 2017

Figure 6. Total CO concentration (molecules/cm^2) retrieved from AIRS. The maps are plotted every two days during 11 and 29 August 2017.

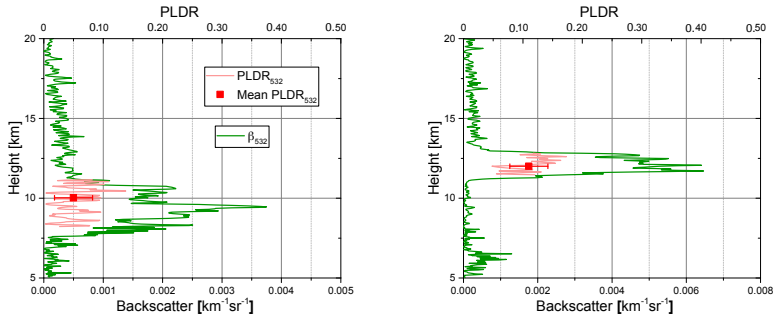

(a) **a** (61.47°N, 106.44°W), 14 August

(b) **b** (62.79°N, 91.54°W), 15 August

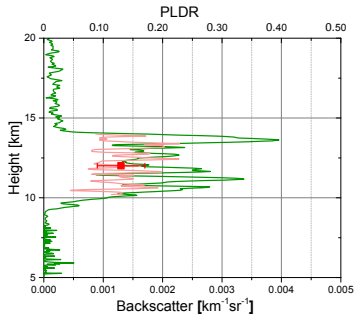

(c) **c** (46.97°N, 72.22°W), 17 August

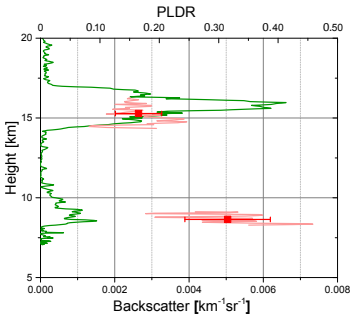

(d) **d** (42.27°N, 42.08°W), 19 August

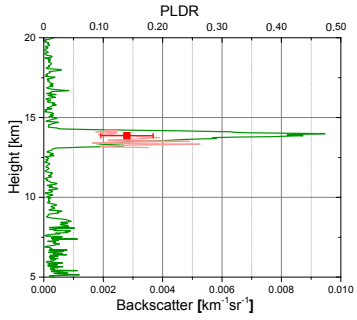

(e) **e** (55.97°N, 12.54°W), 21 August

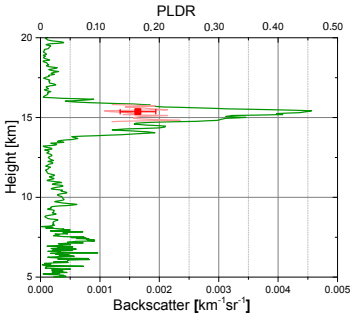

(f) **f** (52.37°N, 13.47°E), 23 August

Figure 7. The profiles of backscatter coefficient and particle linear depolarization ratio (PLDR) at 532 nm from CALIPSO. Figure (a)-(f) correspond to the six locations **a** – **f** in Figure 4. The corresponding CALIPSO tracks are (a) 09:50:19, 14 August 2017; (b) 08:54:37, 15 August 2017; (c) 07:03:13, 17 August 2017; (d) 06:50:44, 19 August 2017; (e) 03:20:25, 21 August 2017 and (f) 01:29:01, 23 August 2017. 20 profiles are averaged over these six locations. The green and pink solid lines represent backscatter coefficient and particle linear depolarization ratio, respectively. The red squares with error bars represent the mean particle linear depolarization ratio and the standard deviation within each layer.

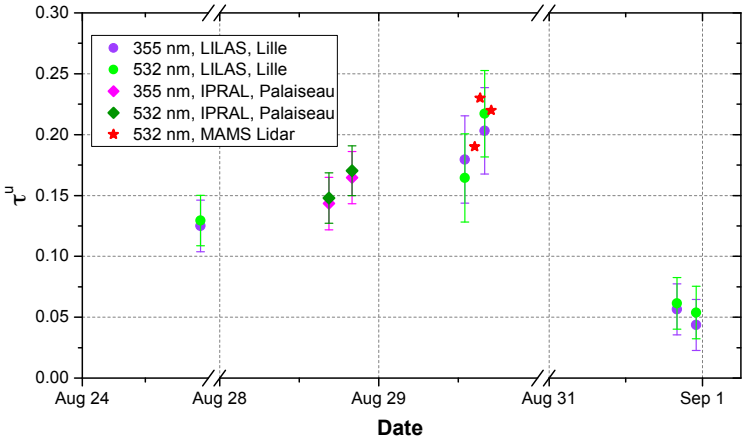

Figure 8. Optical depth of the stratospheric smoke layer at 355 and 532 nm estimated from Lidar signals in August 2017. The optical depth estimated from LILAS (in Lille) is plotted with green (532 nm) and violet solid circles (355 nm). Optical depth calculated from IPRAL (in Palaiseau) is plotted with dark green (532 nm) and magenta (355 nm) solid diamonds. The red stars represent the optical depth calculated from the MAMS Lidar.

Table 2. Retrieved Lidar ratios (LR) and particle linear depolarization ratios (PLDR) from multi-wavelength Lidar systems LILAS in Lille and IPRAL in Palaiseau. $\bar{\alpha}$ is the mean extinction coefficient in the stratospheric smoke layer. ΔL is the thickness of the stratospheric smoke layer. The values after '$\pm$' represent the error of the quantity. Error estimation is presented in the Appendix.

Lidar system	LILAS, Lille					IPRAL, Palaiseau
Date	24 August	29 August		31 August		28 August
Time (UTC)	2200 – 0030	1300 – 1600	1600 – 1800	2000 – 2300	2300 – 0200	1920 – 2120
ΔL (km)	1.0	3.0	3.4	1.4	1.3	2.3
$\bar{\alpha}_{355}$ (km^{-1})	0.12	0.06	0.06	0.04	0.03	0.08
$\bar{\alpha}_{532}$ (km^{-1})	0.14	0.06	0.06	0.04	0.03	0.08
LR_{355} (sr)	35 ± 6	45 ± 9	41 ± 7	34 ± 12	31 ± 15	36 ± 6
LR_{532} (sr)	54 ± 9	56 ± 12	54 ± 9	58 ± 20	58 ± 23	58 ± 7
$PLDR_{355}$	0.23 ± 0.03	0.24 ± 0.04	0.24 ± 0.04	0.28 ± 0.08	0.28 ± 0.08	0.27 ± 0.05
$PLDR_{532}$	0.20 ± 0.03	0.18 ± 0.03	0.19 ± 0.03	0.18 ± 0.03	0.18 ± 0.03	–
$PLDR_{1064}$	0.05 ± 0.01	0.04 ± 0.01	0.05 ± 0.01	0.05 ± 0.01	0.05 ± 0.01	–

Reply To: The mean extinction coefficients are added in the table, refer to AA **A7.** , AA **A21.**

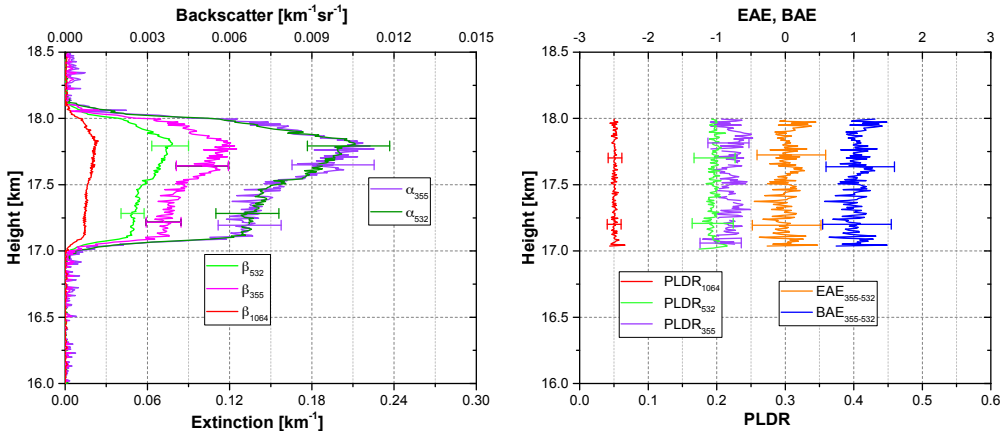

(a) (b)

Figure 9. (a) Extinction and backscatter coefficient, (b) particle linear depolarization ratio (PLDR), the extinction-related Ångström exponent (EAE) and backscatter-related Ångström exponent (BAE) retrieved from LILAS observations between 2200 UTC, 24 August 2017 and 0030 UTC, 25 August 2017, Lille. The errors of extinction, backscatter coefficient and corresponding Ångström exponent at 355 and 532 nm are attributed to the error of the optical depth.

Table 3. Retrieved microphysical properties using the Lidar data in Lille and Palaiseau. Extinction and backscatter coefficients shown in Figure 9(a) and 10(a) are averaged in the range of 17–18.0 km and 17.5–19.5 km, respectively. The averaged extinction and backscatter coefficients are used as the input of regularization algorithm to retrieve particle microphysical properties.

	R_{eff} (μm)	V_c $(\mu m^3 cm^{-3})$	m_R	m_I
Lille, 24 August	0.33 ± 0.10	22 ± 8	1.55 ± 0.05	0.028 ± 0.014
Palaiseau, 28 August	0.33 ± 0.10	15 ± 5	1.52 ± 0.05	0.021 ± 0.011

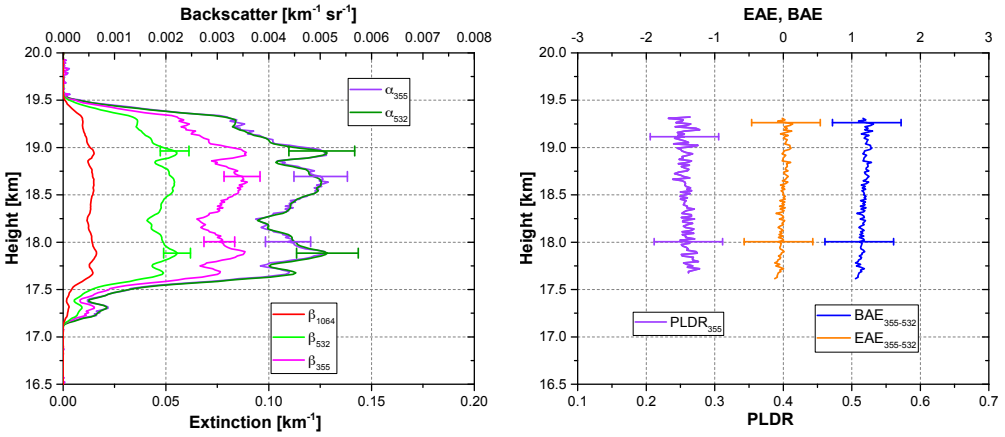

(a) (b)

Figure 10. (a) Extinction and backscatter coefficient, (b) the particle linear depolarization ratio (PLDR) at 355 nm, the extinction-related Ångström exponent (EAE) and backscatter-related Ångström exponent (BAE) (between 355 nm and 532 nm) retrieved from IPRAL observations between 1920 and 2120 UTC, 28 August 2017, Palaiseau.

Table 4. Daily averaged net DRF flux calculated by GARRLiC/GRASP. Aerosol microphysical properties in Table 3 and aerosol vertical distributions in Figure 9(a) and 10(a) are used to calculate the DRF effect at the following four vertical levels.

ΔF (W/m^2)	TOA	BOA	layer top	layer base
Lille, 24 August	-1.2	-12.3	-2.1	-12.0
Palaiseau, 28 August	-3.5	-14.5	-2.5	-13.6

Reply to Anonymous Referee #1:

Thanks to the reviewer for his/her helpful advice, please find our answers below:

Received and published: 4 August 2018

GENERAL COMMENT

The paper presents an interesting study on long-range transported smoke aerosols, originated in Canada wildfires, in the UTLS (Upper Troposphere/Lower Stratosphere) over Europe detected at several EARLINET stations in summer 2017 in combination with satellite observations. Optical depth at 532 nm from 0.05 to above 0.20 were detected, with very weak spectral dependence. Other particle microphysical properties like Lidar ratio and particle depolarization ratios suggest the presence of aged smoke likely with complicated morphology. The retrieved aerosol properties allowed the computation of the direct radiative forcing (DRF) effect originated in the UTLS aerosol layers and the radiative heating rates in this layers that are coherent with the observed radiosonde temperature profiles. The paper is worthy to be published in ACP having in mind that evidences the capabilities of a lidar network focused on tropospheric research in obtaining valuable information on the UTLS aerosols. For this purpose both the advanced instrumentation and the analytical tools used are crucial. The paper is well written and offers valuable information for the reader. Nevertheless the clarification of some points will enhance the quality of the paper.

PARTICULAR COMMENTS

In this work it is especially relevant to get information on the accuracy and uncertainties of the retrievals. The AOD retrievals and the lidar ratio retrievals are clearly related in the analysis procedure used. In this sense, the approach followed for the computation of the UTLS AOD and Lidar ratio with the fixed lidar systems is stated and details on the error propagation and discussion on the accuracy and uncertainty of the retrievals is presented. Nevertheless, some points require additional clarification.

1. Thus, concerning the discussion on the error propagation, in Page 7, I have a question: Are the authors assuming the absence of errors in the molecular part? Having in mind the impact of an accurate thermodynamic profile on this assumption I do not see any information on the thermal profile used. Furthermore, although the computation of the uncertainties is applied in the analysis sections, it would be worthy to include some quantitative information concerning the final uncertainties of the UTLS AOD and UTLS lidar ratio retrievals in the last paragraph in section 3.1.1.

A1: The temperature and pressure profiles are taken from radiosonde measurement in the closest stations: Trappes 20 km from Palaiseau and Beauvechain 120 km from Lille

station. Although the radiosonde stations are not exactly collocated with the lidar observations, we found the spatial variations are minor after exanimating the variability of the temperature and pressure profile in the two stations in August 2017. We think the errors resulting from molecular scattering are not significant, so it is not considered in the total error estimation of the optical depth.
The total error is calculated following Equation (4) and (5), and the calculation process is quite straightforward, we think that it is not necessary to present the calculation details in the paper.

2. In the case of the MAMS lidar retrievals there are additional limitations and the issue of accuracy and uncertainty is particularly relevant. Thus, in spite of the auxiliary use of its data, it is necessary to include additional discussion on the reduced accuracy of this retrieval.

A2: The limitation of MAMS lidar inversion is discussed in the 'Methodology' section before the MAMS results are presented. In the revised version, we mention when presenting MAMS results, that "the MAMS results are limited mainly by the difficulty of quantifying the errors resulting from the lidar signal at high altitude and the assumption of vertically constant lidar ratio".

3. Considering the uncertainty in the AOD retrievals the AOD spectral dependence will present a large uncertainty that requires additional discussion.

A3: The error of the Angstrom exponent Å is derived from the following equation:

$$(\Delta\text{Å})^2 = \left(\frac{1}{\log\left(\frac{\lambda 1}{\lambda 2}\right)}\right)^2 \left[\left(\frac{\Delta\tau_{\lambda 1}}{\tau_{\lambda 1}}\right)^2 + \left(\frac{\Delta\tau_{\lambda 2}}{\tau_{\lambda 2}}\right)^2\right]$$

Considering the error of the two selected cases, the error of optical depth is about 10%, the estimated error of the Angstrom exponent is about 0.3 (absolute value, unitless); and if the error of optical depth is 15%, the resulting error of Angstrom exponent is about 0.5(absolute value, unitless). Compared to the extinction coefficient, the backscatter coefficients we derived are more reliable because they are rather consistent with the results from Raman inversions, except the 1064 channel. The main error of regularization input comes from the error in the spectral AOD and the backscatter coefficient at 1064 nm.
The above information is reorganized and added into the revised version.

4. More details about the procedure used in GARRLIC for the computation of the

aerosol DRF and the UTLS, layer heating rates must be provided.

A4: More information has been added in the manuscript to describe the general strategy of GARRLiC /GRASP and the input parameters for the calculation procedure. The theories and methodology of GARRLiC/GRASP can hardly be well presented in a short section. So we suggest the readers to refer to previous publications about GARRLiC or GRASP. GRASP is an **open source algorithm**, anyone who is interested in using GRASP to reproduce the results in this paper or to invert their own measurements, is **very welcome** to download the algorithm here: https://www.grasp-open.com or contact us by email.

Minor changes

5. The references on the EARLINET network must include a recent reference that updates the features of the network: Pappalardo, G., Amodeo, A., Apituley, A., Comeron, A., Freudenthaler, V., Linné, H., Ansmann, A., Bösenberg, J., D'Amico, G., Mattis, I., Mona, L., Wandinger, U., Amiridis, V., Alados-Arboledas, L., Nicolae, D., and Wiegner, M.: EARLINET: towards an advanced sustainable European aerosol lidar network, Atmos. Meas. Tech., 7, 2389-2409, https://doi.org/10.5194/amt-7-2389-2014, 2014.

A5: It is added.

6. Please consider the following reformulation of the statement on Page 6 Line 2 "at this temperature clouds consist mainly of ice crystals" In order to increase the clarity of the test include the following changes in the first paragraph of section 3.1.1: Substitute:" The integral of the extinction coefficient over the UTLS layer, expressed below, is compared with the pre-calculated optical depth" by "The UTLS AOD is calculated by the integral of the extinction coefficient over the UTLS layer, expressed below". And after equation (2) reformulate the statements: "This pre-calculated optical depth is derived from the elastic channel at 355 and 532 nm. The method is widely used in cirrus clouds studies (Platt, 1973; Young, 1995). " as follows" by "This derived value of AOD is compared with the pre-calculated optical depth obtained from the elastic channel at 355 and 532 nm using a method widely used in cirrus clouds studies (Platt, 1973; Young, 1995)" In page 7 Line 7 change: "We calculate the signal mean within a window of 0.5 km..." by "We calculate the lidar signal mean within a window of 0.5 km. . ." In page 9 line 13 consider changing "intervals" by "periods".

A6: These statements are re-phrased; some are not exactly modified as suggested but in a similar manner.

Reply to Anonymous Referee #2:

Thanks a lot to the reviewer for his/her helpful advice. Please find our point-by-point response below.

Received and published: 8 August 2018

General assessment and major comments

This study provides lidar measurements from two sites in Northern France, showing long range transported smoke in the UTLS. The absorbing nature of smoke is crucial for the stratospheric height ranges, concerning both heating rates (HR) and direct radiative forcing (DRF). The authors try to estimate the DRF and HR and their results show decrease of the radiation reaching the surface and an increased HR due to the absorption of the solar radiation at TOA. In general, I find this study very interesting and of high value. It is a study that fits well in the EARLINET special issue, since it demonstrates the value of EARLINET lidars for atmospheric research in both troposphere and stratosphere. However, before proceeding with publication in ACP, I strongly suggest that the authors would revise the following points:

1. Page 11, Lines 18-27: "The spheroid model was used to retrieved dust properties (Dubovik et al., 2006; Mishchenko et al., 1997; Veselovskii et al., 2010). But it is not clear if this model is applicable to soot particles with complicated morphology. The size of smoke particles is expected not too big so that we choose to apply regularization algorithm with sphere model." The retrieved microphysical properties seem to be associated with high uncertainties, since the shape used (spherical) does not reproduce the depolarization measurements and it should not reproduce accurately the backscattered light measurements either. The reported uncertainties in Table 2 refer to cases of spherical particles and are not representative. Please provide a better assessment of the retrieval uncertainties.

A1: It is true that spheres do not represent correctly smoke particles, neither spheroid. Our retrievals of dust particles demonstrated, that when spheres were used instead of spheroids, the algorithm was still able to provide reasonable estimates of volume and effective radius (Veselovskii et al, JGR 2010). The main errors were attributed to estimations of the refractive index. So we expect that in the case of smoke estimations of radius and volume are also possible.

2. Regarding the DRF calculations: these are based on the retrieved microphysical (point 1) properties which, as discussed above, are derived from the 3b+2a regularization inversion and are associated with (most probably) high

uncertainties. Especially for the imaginary part this uncertainty is expected to be the highest (Burton et al., 2016). Please provide a better assessment of the retrieved property uncertainties and quantify the uncertainties of the DRF calculations accordingly. If this is not possible, omit section 4.2.3 from the manuscript. This also applies to Page 14, Lines 9-13, where the derived complex refractive index is compared to other studies. Omitting 4.2.3 would not affect the quality of the paper, since the authors already provide important results on smoke optical properties and microphysical estimates.

A2: From our simulation studies we estimate errors of V (volume concentration) and R_{eff} as 30%, for m_R it is +-0.05 and m_I 50%. These are typical values and we are not able to evaluate the effect of shape of on retrievals. But basing on dust studies, we expect it to be similar.

The deficiency of using sphere model is its not being able to reproduce the depolarization effect. However, the estimation of the radiative effect is not so sensitive to the depolarizing effect of the particles. Indeed, the uncertainty of the imaginary part of the complex refractive indices is much higher than the other parameters and it is strongly dependent on the shape of the particles, but the values we present are quite reasonable for previously reported absorbing smoke. We think the estimated radiative forcing is quite representative and the heating of smoke predicted by the DRF is able to explain the ascending trend of the plume, as shown in the newly added figure. Although the values suffer from some extent of uncertainties, we would like to keep section 4.2.3 and we will mention in the manuscript that the uncertainty of the retrieved aerosol microphysical properties affects the accuracy of the DRF estimation.

3. Another issue addressed in this study is the increase in particle depolarization ratio at 532 nm which is attributed to the particle aging. The authors gathered observations of the particle linear depolarization at 532nm from previous studies and have also included the results obtained from the present study. Nevertheless, the only visible trend seen in Figure 11 results from CALIPSO measurements. From the ground-based lidars in Lille and Palaiseau, there is no obvious increase at 532nm. In conclusion, the phrase“we found an increase in depolarization versus transport time” in the manuscript abstract should be changed to “CALIPSO observations of the UTLS smoke layer suggest an increase in depolarization at 532nm versus transport time”.

A3: We agree that the main increasing trend of the depolarization is indicated by the CALIPSO measurements. However, the CALIPSO data are questionable because of the high noise level. Moreover, the RH of the smoke plumes is not known. As a result, we cannot draw really convincing conclusion about the changes of depolarization ratio

during the aging process. At current stage, we decide to remove this part from the manuscript and more efforts will be made to investigate this issue and re-assess CALIPSO data.

Minor comments

4. Page1, Line 9: “Typical particle depolarization” the meaning of the word typical should be clarified by the authors, meaning what is the definition of linear particle depolarization ratio used? (is it the cross/parallel ratio or the cross/total ratio?)

A4: After re-organizing the paper, the definition of particle linear depolarization ratio is in Section 2. The methodology is presented before the observation section, so this problem is avoided.

5. Page 1, Line 10: “The relatively high depolarization ratios and such spectral dependence are an indication of a complicated morphology of aged smoke particles” The conclusion that the spectral dependence of the depolarization ratio is characteristic of aged smoke particles can be hardly drawn by two cases, i.e. the current one and the one reported in Burton et al. (2015). Please rephrase accordingly.

A5: This conclusion is drawn in Mishchenko et al., 2016

6. Page2, Line 30: “We focus on the retrieval of the aerosol optical and microphysical properties from the Lidar measurements”. The authors should highlight that the depolarization ratio values are not reproduced in the retrieval of the microphysical properties.

A6: Yes, this message is given in section 4.2.3 as the limitation of the retrieval.

7. Page 4, Line 2: Please change the phrase “showed an increase of temperature in the stratospheric smoke layers” to “An increase of temperature due to the presence of smoke aerosols in this region” or something similar.

A7: Modification has been made in the revised manuscript.

8. Page 5, Line 3: Change the phrase “A plume with relatively high UVAI first occurred over the British Columbia on 11 August, and the intensity of the plume was moderate” to “a plume of moderate intensity and relatively high UVAI, first occurred over British Columbia on 11 August. Page 5, Line 4: Please change the phrase “and the UVAI in the center of the plume reached above 10” to “and the

UVAI in the center of the plume reached above 10, as indicated by the grey area on the plot (Fig 4)"

A8: Modification has been made in the revised manuscript.

9. Page 6, Line 1: "We have examined the temperature profiles" Did you use radiosonde measurements? Please provide more info.

A9: Yes, it is radiosonde measurements from Wyoming radiosonde stations, data can be found here: http://weather.uwyo.edu/upperair/sounding.html

10. Page 6, Line 2: "the temperature drops below -38_C, at which temperature the cloud droplets mostly turn to ice phase" Please provide relevant reference.

A10: Please refer to Kârcher et al., 2003, A parameterization of cirrus cloud formation: Heterogeneous freezing.

11. Page 6, Line 8: "The increasing trend of the depolarization ratio is probably due to aerosol aging" As discussed above, this is a hardly drawn conclusion. Please rephrase accordingly.

A11: We decide to remove this argument.

12. Page 7, Line 7: "we can calculate the optical depth of the cirrus cloud" Please change "cirrus cloud" to "UTLS aerosol layer" since this is what you refer to in this case.

A12: Corrected.

13. Page 7, Line 12: change the phrase "are considered as the major error sources of the optical depth" to "are considered as the major error sources in the estimation of the optical depth"

A13: Corrected

14. Page 7, Line 13: "based on the statistical error of photon distributions" Please provide more info on the definition of the noise of your lidar measurements. Do you take into account the systematic errors?

A14: The error of the lidar signal is estimated based on the assumption that the photon-counting detection mode of the photomultiplier follows Poisson distribution. Then signal error is given by the covariance of the Poisson distribution. Systematic error of photon-counting detection is negligible especially in nighttime measurements, so it is not taken into account in the error estimation. We estimated about 3% of error for nighttime signal. In order to account for the interference of sunlight, we roughly use 5%

for the error in daytime.

15. Page 7, Line 22: change the phrase “of the error of optical depth” to “of the error of optical depth to the estimation of the Lidar ratio”

A15: corrected

16. Page 10, Line 15: typing error, change volume depolarization ratio at 355 nm to molecular depolarization ratio at 355 nm.

A16: Corrected

17. Page 14, Line 14: “Smoke in dry conditions have higher refractive indices than that in wet condition” Provide relevant reference.

A17: After reconsideration, we think this statement is not strict. Studies have shown that fresh smoke has a broad range of hygroscopicity. The study of the hygroscopicity of aged smoke is quite limited and requires more observational and experimental efforts. Additionally, the aging process could be very complicated considering possible effects related to the photochemical process, fuel types, particle coagulation, secondary aerosol generation and so on.

We decide to remove this comment and mention in the revised manuscript that “the hydroscopicity of aged smoke is not yet well revealed.”

18. Figure 6: The x axes on CALIPSO plots should be the same in order to show the variation. Also the phrase in the caption “The profiles of backscatter coefficient and particle linear depolarization ratio (PLDR)” could be changed to “The profiles of backscatter coefficient and particle linear depolarization ratio (PLDR) at 532nm from CALIPSO” Figure 7: The points on this figure should be larger to be more visible. Also, it would be better if the colors of the points are different for the two lidar systems.

A18: Corrected.

Response to Anonymous Referee #3 :

Thanks a lot to the reviewer for his/her helpful advice. Please find our point-by-point reply below.

Received and published: 17 August 2018

The paper provides unique measurements of an extreme event of smoke advection from Canada to Europe. Smoke could be observed within the Troposphere as well as in the Stratosphere. I consider the measurements and the resulting data as very valuable and of interest for the scientific community and the topic fits well in the scope of ACP.

However, in my opinion the paper tries to cover too much topics at once (optical properties of smoke, microphysical properties, source analysis, change of depolarization with aging time by using Calipso data, radiative transfer calculations, estimating of heating rates, temperature changes in the stratosphere etc.). Thus, the paper is partly confusing and for some of the topics the proper fundament needed for the conclusion drawn are missing.

I therefore recommend first to focus on your key expertise and present only the unique measurements, which are already shown and exploit as much as possible (optical and inversion results). Of course you should also include the satellite data for source analysis. However please focus on the lidar measurments in France. Then, in another paper(s), the other topics could be covered (i.e. radiative transfer calculations and heating rates etc.) Especially the discussion of the impact of the smoke plumes need much more detail and evidence, as for example it is not shown nor discussed that temperature increases in the stratosphere at a certain height are not caused by the complicated upper atmospheric circulation including tropopause foldings etc. I therefore recommend for the second paper to include some expertise of the upper atmospheric dynamics and probably some modelling to show and prove the impact of the smoke layer with its possible warming on the overall general condition of the UTLS region above Europe.

I also think that the use of Garrlic/Grasp radiative transfer code to obtain radiative impact must be explained much better. Currently, it is not understandable how the calculations are performed.

From the current version, I also doubt for the evidence of the increase in smoke depolarization with aging time. I think the use of Calipso data for such a study is again a topic of its own. Uncertainties in the Calipso retrieval (see comments in pdf) should be discussed. Even more important, other influencing factors as the relative humidity, the altitude of the smoke with respect to ground level but also tropopause should be investigated. Among others influencing factors (fire source, burning types).

I therefore recommend major revision with the recommendation written above. Find

other comments below and as pdf-comments in the supplement.

Paper structure:

1. -The abstract is too long. Please shorten.

A1: The abstract is rewritten after all the corrections.

2. -The introduction is in my opinion a loose sequence of different paragraphs and therefore not constructive. Please revise and make it more focusing on your topic. E.g.: have such events been reported earlier? Is this the first time? . . .

A2: Modifications have been made.

3. -Several facts concluded in the observations section are again raised in the discussion. I think you should shape your paper. Either describe your observations only, and then make a discussion in a separate section or make conclusions also in the observations section but then discuss only new issues in the discussion section.

A3: The abstract, introduction, discussion as well as the conclusion have been re-shaped.

Terminology

4. -I would recommend not to use "upper troposphere/lower stratosphere UTLS" as a standard the term. This historical term covers all altitudes between 5 and 30 km and thus does not make clear that a significant portion of the smoke you detected is above the local tropopause. Please feel free and state, that there is stratospheric smoke as well as smoke in the free troposphere. In most times you anyhow refer to stratospheric smoke with your statements. . .

A4: We decided to change "upper troposphere/lower stratosphere UTLS" to lower stratosphere.

Major scientific remarks:

5. -What about the uncertainties of Calipso. For example for the PLDR, the particle backscatter coeff. is needed which is in turn calculated with a Klett-like approach, i.e. a a-priori lidar ratio. Thus the questions arises, which aerosol type was classified by Caliop and which lidar ratio was used to obtain the PLDR and is this correct for your aerosol type of investigation.

A5: This is a very useful comment. In Figure 6, we find that the observed plumes are not well classified. 1) The classification provides scattered aerosol types, such as polluted dust, elevated smoke, dust and volcanic ash. 2) The derived aerosol type sometimes

oscillates profile by profile, and even adjacent profiles could be classified into different categories. Different aerosol types correspond to different lidar ratio assumptions, but Figure 6 shows the mean profiles of backscatter coefficient and PLDR over a small range (latitude ±0.01), without considering the impact of aerosol mis-classification. In this situation, the error of CALIPSO results is barely expectable.

We added in the manuscript that the plumes are not well classified in CALIPSO data processing and this decreases the accuracy of CALIPSO results. But we still keep Figure 6, in order to the transport of the smoke plume from Canada to Europe. In addition, we remove the argument about PLDR increasing with transport time, because of the unknown error level of CALIPSO PLDR product.

6. -Depolarization: The molecular depolarization ratio depends on your filters used in the lidar. Are the theoretical values you stated valid for your system? And can you neglect temperature effects? Which molecular depol ratio value did you use for the PLDR calculation? The measured one or the theoretical one?

A6: The theoretical value of molecular depolarization ratio (specific to the Cabannes line) is about 0.36%. However, due to the imperfection of the lidar optics (and ther factors), the measured depolarization ratio in the aerosol-free zone is higher than the theoretical value. Our interference filters in LILAS system well block the rotational Raman lines. Figure 1 below shows the rotational Raman lines and Cabannes lines for the laser wavelength at 532 nm (in standard atmosphere), as well as the transmission function of the interference filters. We have estimated the total molecular depolarization ratio to be 0.4%, including the Cabannes lines and rotational Raman lines and found that the impact of the included rotational Raman lines on the molecular depolarization ratio is quite minor. However, in the historical measurements, our system LILAS measured about 0.8—1.3% at 532 nm, 1.2—1.8% at 355 nm and 0.7—1.0% at 1064 nm. The depolarizing effect of the optics, the misalignment and the error in the calibration procedure are expected to be responsible for the error of measured molecular depolarization ratio. In the calculation of the aerosol particle linear depolarization ratio and its error, we use 0.4% for the molecular depolarization ratio. The error level of molecular depolarization may look a bit astonishing but, fortunately, the total error of the particle depolarization ratio is much less dependent on it when the aerosol is optically thick and depolarizing, like in the presented cases. In addition, we measured cirrus clouds below the stratospheric plumes on 24—25 August, the derived PLDRs are about 45%, without noticeable spectral dependence. The results are very consistent with previously reported PLDR of ice clouds and can be regarded as a verification of our measurements.

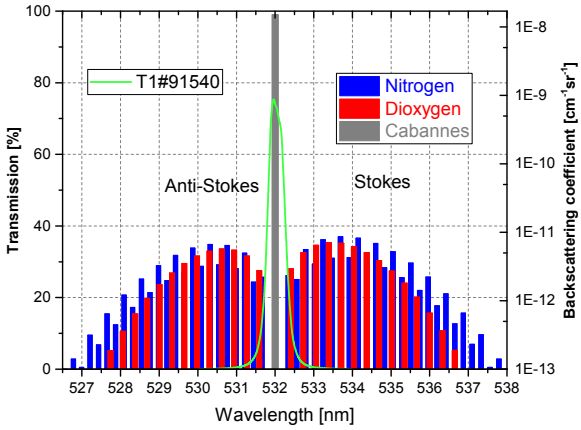

Figure 1. The molecular backscatter coefficient of rotational Raman lines and Cabannes line for the laser line at 532 nm. The calculation is made under a standard atmosphere. Only oxygen and nitrogen are considered as scatters in the atmosphere.

7. -Radiative transfer: The methodology explanation is too short. It is not reproducible how you performed the radiative transfer. Which parameters did you use as input? Which are constrained by the algorithm? and so on... thus, either you introduce a much more detailed description of this method and the paper gets longer or you shift these calculations to a second paper.

A7: We agree that the explanation about GARRLiC/GRASP is not enough for reproducing the forcing effect of the smoke plumes. More information has been added in the manuscript to describe the general strategy of GARRLiC /GRASP and the input parameters for the calculation procedure. The theories and methodology of GARRLiC/GRASP can hardly be well presented in a short section. So we suggest the readers to refer to previous publications about GARRLiC or GRASP. GRASP is an **open source algorithm**, anyone who is interested in using GRASP to reproduce the results in this paper or to invert their own measurements, is **very welcome** to download the algorithm here: https://www.grasp-open.com or contact us by email.

8. -Inversion: Is it useful to perform an inversion when having only 3 elastic signals? I mean lidar ratio is not an independent variable in your case...please discuss this!

A8: The lidar ratio is not a completely independent parameter, because we introduce an extra constraint, which is the optical depth of the smoke layer. Indeed, assuming vertically constant lidar ratio is not a favorable way in the Raman lidar community,

because it looks not realistic in some cases. But do not forget that, the particle depolarization ratio is almost vertically constant in the smoke layer. It indicates that the particles are well mixed in the smoke layer. Based on this fact, we have confidence to say that the lidar ratio within the smoke layer will not show significant variations. To assure this hypothesis, we compared the backscatter coefficient calculated from Raman and Klett method. The comparison in the selected two cases is shown in Figure 2. One can see that the differences in the backscatter profile between the two methods are quite minor. It indicates that the backscatter coefficient we calculated is reliable and assuming a constant lidar ratio in the smoke layer is not far from the truth.

There are actually **5 input parameters** in regularization algorithm. As to the extinction profile, it fits the pre-calculated optical depth so the mean extinction in the smoke layer is also trustworthy.

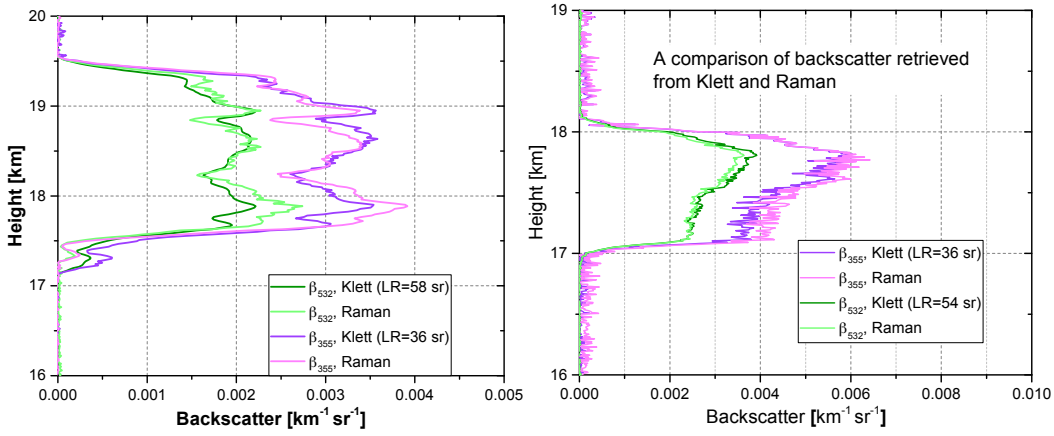

Figure 2. The comparison of backscatter coefficient, (left) 19:20—21:20 UTC, 28 August 2017, Palaiseau and (right) 20:30—00:30 UTC, 24—25 August 2017, Lille

9. What justifies using a sphere model when particle size is small.

A9: It is maybe a bit miss leading to say that the small particle size justifies the applicability of sphere model. What we really wanted to address is: the difference between spheroid scattering and sphere scattering is very minor when the particle size is small, and to not complicate the situation, we chose to use a simpler model, the sphere model.

The sensitivity of scattering of particles to the shape (spheres or spheroids) can be found in "*Dubovik, O., et al. (2006), Application of spheroid models to account for aerosol particle nonsphericity in remote sensing of desert dust*". Figure 3 is taken from

the Figure 26(b) in Dubovik et al. 2006. It plots the lidar ratio at 532 nm as a function of the aerosol Angstrom exponent, which is an indicator of the particle size.

It can be seen that when the Angstrom exponent gets bigger, the difference of lidar ratio between spheroid and sphere model gets smaller.

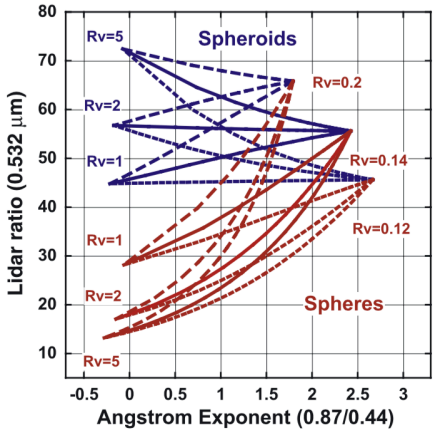

Figure 3. Lidar ratio plotted as function of Angstrom exponent. Rv is the mean radius of the size distribution. Each line shows the dependence of the lidar ratio for aerosol defined by a lognormal bimodal distribution of spherical (red labels) fine mode (with median radii 0.12, 0.14 or 0.2 mm) and coarse spherical (red labels) or spheroid mode (blue labels) (with median radii 1.0, 2.0, 3.0 or 5.0 mm).

10. -Increase in stratospheric temperature. Your explanations are not convincing concerning the temperature increase. Did you consider also all other processes in the UTLS? May this only be normal variability? How long do you observed a temperature increase? So please add more detail or shift to another paper (I think this is a topic alone).

A10: Other process, for example the variation of ozone concentration can also result in temperature changes in the stratosphere. We investigated the temperature profile measured by radiosonde at Trappes (close to Palaiseau, France) in the last two weeks of August 2017. Figure 4(a) shows that the temperature in the stratosphere has obvious variations in August 2017. The region in the magenta box is distinct with others, because it is an obvious local maximum. Moreover, the spatial-temporal occurrence of this temperature peak coincides with the occurrence of the smoke plume. The same spatial-temporal coincidence appears to Beauvechain temperature observation (close to Lille station). Based on the observations in two independent observation site, we are confident that temperature increase in the plume layers is caused by the presence of the absorbing smoke layers instead of other reasons.

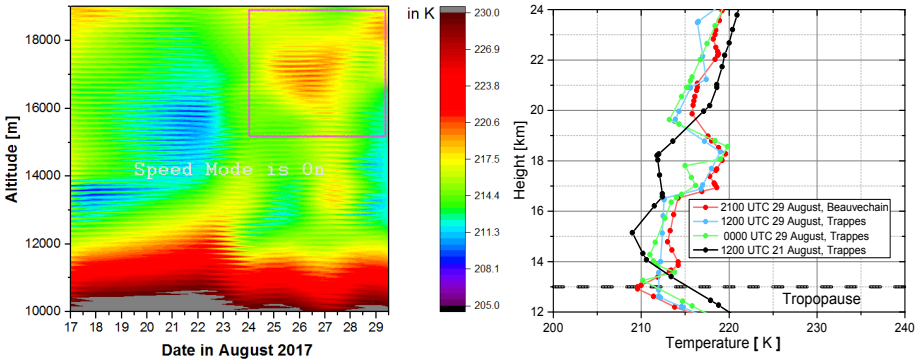

Figure 4. (a) Temperature at Trappes in August 2017. (b) Temperature profiles at Trappes and Beauvechain.

11. -Depolarization ratio vs. aging time: The provided graphic and literature review does not convince me of the given causality, please also investigate the RH, the height etc. vs depolarization ratio.

A11: We agree that CALIPSO data are very noisy from which we can hardly draw convincing conclusion about the depolarization increasing with aging time. The error level of CALIPSO measurements is also questionable regarding the stratospheric smoke layers. In addition, the RH of the smoke plume is not available in CALIPSO measurements and some ground-based lidar observations. As a result, we decide to remove the questionable argument about depolarization increasing with aging time. We need more investigations before getting more convincing results.

- Please also note the supplement to this comment: https://www.atmos-chem-phys-discuss.net/acp-2018-655/acp-2018-655-RC3- supplement.pdf

The modifications as below have been made following the comments in the supplement:

1. The abstract, introduction discussion and summary are reshaped.
2. Typing and grammatical errors, ambiguous statements and other minor errors pointed out by the reviewer have been corrected.
3. A table has been added to summarize the configuration of the three Lidars

4. Data will be uploaded to EARLiNET database after the final review session. More

information about data availability is added.

5. Acknowledgement is modified and author contribution is included.

6. Errors of Rayleigh scattering?

AA6: We use temperature and pressure profiles from the closest radiosonde profiles. The Rayleigh fit in the aerosol free zone is excellent so the errors resulting from molecular scattering are ignored in the error estimation.

7. Why not simply use the lidar ratio you retrieved with the other method or the ones reported by Haarig et al.? I consider using the total AOD as a constrained much more critical as you have to use one lidar ratio for all heights...you could also use the lidar ratio of the PBL obtained with LILAS or IPRAl for the MAMS Klett retrieval in the PBL.

AA7: MAMS system performed measurements between Palaiseau and Lille. There are three data points from MAMS, two of them are not collocated with IPRAL or LILAS, and only the third data point was obtained in Lille. We lack the information of the tropospheric aerosol along the road. Moreover, considering the noise in MAMS lidar daytime measurements, the AOD measurement collocated with the MAMS Lidar should be a more solid constraint. So we chose to process MAMS lidar measurements with an extra constraint of AOD.

8. Divide the paper into two papers

AA8: After re-shaping the paper and considering the advise from the other reviewers, we would like to keep the observation, inversion and radiative forcing estimation in the same paper. But, as you suggested, we added more information about GARRLiC/GRASP algorithm. We cannot present all the details about GARRLiC/GRASP because it is an integrated algorithm containing many modules. In the revised version, the basic strategies and the input parameters are introduced in more detail, so if the users want to reproduce the results, they can download this open-source algorithm and follow the instructions. The information we present in the paper is to show the general strategy of the algorithm.

Reply to Albert Ansmann:

Thanks a lot for this very detailed and helpful review. Please find our point-by-point answers below:

General remark:

The paper is well written and focuses on an interesting atmospheric topic: Long-range transport of pyro-cumulonimbus-related Canadian fire smoke in the stratosphere observed over France in August 2017.

An original and unique measurement strategy is selected: Two lidars at Palaiseau and Lille and one mobile system that measured the smoke during a travel from Palaiseau to Lille.

The highlight is the retrieval of the spectrum of the particle linear depolarization ratio measured at three wavelengths. There is a strong decrease of the depolarization ratio from 25% in the UV down to less than 5% in the near IR.

However, the discussion of the results is partly confusing and must be improved. Major revisions are necessary. Detailed comments:

1. *The title is misleading. The focus is on lidar observations (in France) of aerosol layers several kilometers above the tropopause, and not below the tropopause (upper troposphere). So: ... smoke aerosols in the lower stratosphere .... would be correct. Furthermore, the title does not indicate where you made these observations: .... Long range transport of Canadian fires smoke towards Europe observed over northern France ... , and not, for example, in eastern Asia or in the Arctic. Please improve!*

A1: We agree that the plumes shown in this paper are all in the lower stratosphere. We thought that 'Upper troposphere and Lower stratosphere' could be more recapitulative because of the variation of the position of the tropopause.

Considering this suggestion, we changed the title to **'Long-range transported Canadian smoke plumes observed in the lower stratosphere over northern France'**.

2. *P1: The abstract must be updated after the requested changes.*

A2: it has been updated in the revised version

3. *P2, L2: All abbreviations must be explained when they are mentioned for the first time (in the main text). The abstract is a stand-alone text, and does not count in this respect*.

A3: it has been corrected in the revised version

4. *P2, L25. After the foregoing paragraph, a paragraph is missing in which the literature is reviewed which is already available regarding the Canadian smoke period in August 2017: Khaykin et al. (GRL, 2018), Ansmann et al. (ACP, 2018), Haarig et al. (ACP, 2018). If there are more, please mention them as well. Such a literature of foregoing work is (always) required in the Introduction. What is already done and thus known? What is our new contribution?*

A4: it has been done in the revised version

5. *P3, L1.... : Again, please explain: LILAS, IPRAL, PLASMA, MAMS etc...*

A5: it has been done in the revised version

6. *It is quite confusing that Section 2, that contains first observations and in-depth analysis of all the satellite observations of the smoke including CALIOP (space lidar) measurements, ... is then interrupted by a 'dry' lidar methodology section. It would be better to have the technical*

section first (as section 2, or as an Appendix) and then all the observations and discussions in the follow-up sections, continuously in sections 3, 4, 5.... without a break...

A6: We agree that the 3rd section about methodology and calculation looks like an interrupt, so it has been moved to the 2nd section.

7. *P3, L28: With the AOD of the smoke layer and the vertical extent of the layer (from the lidar observation), the layer mean particle extinction coefficient can be determined. These values should be presented as well.*

A7: The mean extinction coefficients have been added into the table.

8. *P4, L13: Please explain EOS AM-1*

A8: EOS means 'Earth Observing System'. AM and PM mean the time when the satellite passes over the equator is in the morning or in the afternoon. This information has been deleted in the revised version because it is not so relevant to this study.

9. P4, Section 2.4: Isn't that a similar study of OMPS UVAI maps as already presented by Khaykin et al. (2018, in the supplementary part)? Should be mentioned.

A9: Yes, it is the same results with by Khaykin et al. 2018, products from the OMPS aerosol index are used to trace the evolution of the smoke plumes. Comments have been added in the text.

10. P5, L3: I see a clear and strong jump in the aerosol load from 11 to 13 August 2017 over the northern parts of western North America (Canada), in Figure 4. This is a clear and convincing indication that the pyrocumulonimbus cluster activities on 12 August were most probably responsible for these aerosol features. But this not explicitly written.

A10: Comments have been added in the text.

11. P5, L10: explain AIRS!

A11: AIRS means Atmospheric Infrared Sounder, this has been explained in the introduction part.

12. *P5, L10-25: The same holds for Figure 5, a clear and sudden increase in the CO concentration from 11 to 13 August is visible. Furthermore, this 12 August event seems to be the reason for the extreme smoke load over Europe on 21-22 August (Figure 5f) as reported by Ansmann et al. (2018). This should be also mentioned.*

A12: Comments have been added to explain the increase of CO concentration from 11 to 13 August.

13. P5, CALIPSO section 2.6: You already discuss the linear depolarization ratio, but the definition and explanations are provided later (in section 3). This is one of the reasons, why you better start with a more technical section right after the introduction.

A13: The technical section has been put just after the introduction.

14. P6, L3: Mixed-phase clouds can produce depolarization ratios from almost zero (mainly drops) to 40% (mainly ice crystals), so why should they show depol values of 26-35% only?

A14: We agree that the depolarization ratio of ice clouds is typically about 40%, and mixed-phase clouds in principle should possess a depolarization ratio ranging from a few percent to below 40%. This value, '26-35%', comes from the study of Sivakumar et al., 2003 which is based on the Sassen, 1995. It is based on kind of specific

observational data but does not cover the large variability of mixed phase clouds. We agree to use particle linear depolarization ratio of a few percent to 40% for mixed-phase clouds and above 40% for ice clouds.

15. P6, L8: Why does an increasing trend in the depolarization ratio indicate aging of smoke particles? First of all, I do not see a trend in the noisy CALIPSO measurements. And second, the strong depolarization can be simply explained by the irregular shape of the smoke particles..., and why should the irregular shape change with time in the stratosphere where dry soot particles seem to dominate.

A15: Indeed, CALIPSO data are very noisy and some observed plumes in Figure 6 are not correctly classified, thus introducing unknown errors to the PLDR. We decide to remove the argument about PLDR increasing with transport time.

16. P6, section 3: Interrupt! A complex section is given, which is only interesting for lidar experts. But the paper is written for the research community dealing the atmospheric smoke and aerosols.

A16: This section has been put just after the introduction. In our opinion, it is necessary to present the data processing procedure and the error calculation. We adapted the standard Klett method to avoid an unrealistic assumption of lidar ratio. And this method should be presented to the readers so the results could be reproduced by anyone that is interested in.

17. *In Sect. 2.1, the lidars are explained (Raman lidars). And in Section3, we learn that you make only use of the Klett method. This makes quite a significant difference. The lidar ratios at 355 and 532 nm are not directly measured, you need to assume that the lidar ratio is height constant (and equal to the obtained layer mean value), so the solutions of the backscatter and extinction*

coefficients at a given wavelength are not independent of each other, the profiles are rather similar. And at the end, you use the non-independent extinction and backscatter solutions in the lidar inversion retrieval to obtain the microcphysical properties. This inversion algorithm however needs independently measured backscatter and extinction coefficients at 355, 532 and 1064 nm (backscatter). Please mention and explain this 'contradiction' in more detail. What are the consequences for the inversion uncertainties?

A17: Our observations during this event do not provide optimal data for retrieving extinction coefficient by Raman method. Because 1) for some cases where the plumes' extinction was high (>0.1 km-1), the measurements were made in daytime or with cirrus clouds below the smoke layers; 2) and the other cases where nighttime measurements were made without cirrus contamination, the extinction coefficients of the plumes are quite low. The calculation of extinction coefficient using Raman requires smoothing. The size of the smoothing window and the choice of smoothing method (least-square method is commonly used) is dependent on the Raman signal quality and will certainly impact the retrieved extinction coefficient. The calculation of the backscatter coefficient using Raman method is expected to be less dependent on the smoothing of Raman signal. Indeed, Raman method provide independent calculation of extinction and backscatter, but the smoothing applied on the extinction could introduce some artifacts or 'faked vertical variations' into the lidar ratio profile.

The lidar ratio is a quantity determined by the aerosol type and independent of aerosol concentration, like the particle linear depolarization ratio (PLDR). From the case study in our paper, it can be seen that the PLDR does not show noticeable variations versus altitude in smoke plume in the stratosphere. Neither does the backscatter Angstrom exponent. This is an indication that the smoke particles are well mixed and the properties of the particles are vertically homogeneous within the plume. So we expect that the lidar ratio in the smoke layer do not have strong vertical variations.

Moreover, we apply Klett inversion in the range of (layer_base – 1km) to (layer_top + 1km), to reduce the impact of the assumption of vertically constant lidar ratio.

In addition, we have compared the backscatter profile calculated using Raman method and Klett method, and the differences are quite minor. Please see Figure 2 in this document.

In the revised manuscript, we mention that the backscatter profiles calculated from Klett have been compared with the ones from Raman method (not shown) and they are very consistent. And due the assumption of vertically constant Lidar ratio, the profiles of extinction and backscatter coefficient are similar in the shape.

18. *P7, L7: You calculate the signal means (within 500 m thick layers) at aerosol layer top and base. Please be precise. You probably use signals below the base and above the top only? What happens if there are traces of smoke above and below the layer, what uncertainty causes the use of noisy Rayleigh signals above and below the aerosol layer in the lidar ratio retrieval? All in all, be using the simple Klett method the uncertainty in the lidar ratio values (at 355 and 532 nm) must be at least 30%. All this needs to be clearly stated. We need overall uncertainties in the presented lidar ratios at the end of section 3.1.1.*

A18: We have considered the possible impact of smoke remnants when processing the data. To avoid including any smoke remnants in the base and top window, the two windows are selected in the region that does not touch the base and top of the layer. The Rayleigh fit in the region where the two windows locate is good (in daytime Rayleigh, signal in the top window is inevitably more noisy than in the night), so we are confident that the impact of smoke remnants on Klett inversion is reduced as much as we can do. In the manuscript, we add this sentence: "the window of layer top and base is chosen in a region where lidar signal fits well with molecular scattering profile."

19. The same for section 3.1.2: We need overall uncertainties in the depolarization values at the end of the section. If you have already 10% uncertainty in the volume depolarization ratio at 355 and 532 nm, the uncertainties in the particle linear depolarization ratios will be close to 20% for the particle depolarization ratio (especially at 355 nm). How trustworthy are such very large 355 nm particle depolarization ratios of 28% you present later on in the article? Even in the case of desert dust (rather irregularly shaped particles) the particle depolarization ratio is usually 25% or less. Please comment on this.

A19: The calculation of the overall error of PLDR follows this equation:

$$\left(\frac{\Delta\delta_p}{\delta_p}\right)^2 = F_R\left(\frac{\Delta R}{R}\right)^2 + F_{\delta_v}\left(\frac{\Delta\delta_v}{\delta_v}\right)^2 + F_{\delta_m}\left(\frac{\Delta\delta_m}{\delta_m}\right)^2 \quad (1)$$

where R, δ_v and δ_m represent the backscattering ratio, volume linear depolarization ratio (VLDR) and molecular depolarization ratio. The calculation indicates that the error of the PLDR is mostly determined by the error of the VLDR, especially when R is larger than 10. As shown in Figure below

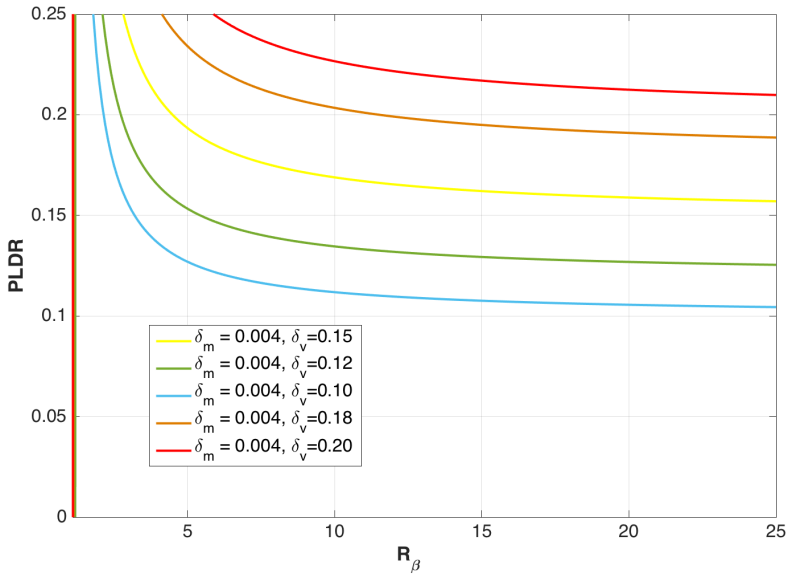

Figure 1. PLDR versus backscatter ratio R

At 355 nm, R is about 3 to 8, considering all the observations we have analyzed. At 532 nm, R is much higher so the error of PLDR depends mostly on the error of VLDR.

For the case where PLDR355 is 28% :

$R \approx 3.5$， $\Delta R=20\%$

$\delta_v \approx 0.15$， $\Delta \delta_v = 10\%$

$\delta_m \approx 0.004$， $\Delta \delta_v = 300\%$

The coefficients of the three terms in Equation (1) are:

F_R=2.28E-01,

F_V=1.15E+00,

F_m= 9.31E-06

And the overall error of the PLDR is about 14.38%.

The calculation process is written in a Matlab script and can be found here: https://www.dropbox.com/s/xjxdg6kxoirb50b/error_depol.m?dl=0

However, we admit that using 15% for the error of PLDR at all the three wavelengths is not quite apposite. Because it is based on the assumption that the error of R is about 20%, but the error of R at 355 nm in the night of 31 August to 01 September is apparently higher than 20%. (15% for PLDR532 is safe enough). We recalculate the error of PLDR355 for the observations on 31 August, with

$R \approx 3.5$， $\Delta R=30\%$

$\delta_v \approx 0.20$， $\Delta \delta_v = 10\%$

$\delta_m \approx 0.004$， $\Delta \delta_v = 300\%$

we obtain about **19%** for the total error of PLDR 355, and by changing ΔR to 50%, we obtain **28%. Thus, we decide to modify the particle depolarization ratio at 355 nm from 28 ±4 % to 28 ±8 % .**

P.S. The error of PLDR532 is still below 15% in this case.

20.*P9, Sect. 4: First question: The given standard deviations (in the text and in Table 1) indicate the uncertainty or the atmospheric*

variability (in time and in the vertical profile) or the uncertainty in the retrieval? It is not clear to me. Please state that clearly. Table 1: I miss the information about the height (base, top) of the smoke layers in the stratosphere in the table. I would recommend providing the layer-mean extinction coefficients as well.

A20: The quantity appearing after the symbol '±' is the uncertainty. Comments have been added in the text to clarify this quantity. And, the mean extinction coefficients of the smoke layer have been added in Table 1.

21.*P10, L15: If you have an uncertainty of 20% in the 355 nm backscatter value and 10% in the volume depolarization ratio then it is hard to get an uncertainty of 15% in the particle depol ratio. I ask this to force you to re-check the results concerning the very large 355 nm particle depolarization ratios of 28%.*

A21: It has been corrected to 28 ±8 %. Detailed explanations are presented in **A19**.

22.P10, L29, Figure 8 and P11, L5: The only reliable profiles are the Klett solutions for the backscatter profiles. The extinction profiles and the EAE profiles are estimates and are strongly based on the used height-constant (layer mean) lidar ratios. It should be made very clear that the solutions of backscatter and extinction are so similar (or better identical in the profile characteristics) because of the use of the Klett method and the assumption of a height-constant lidar ratio. In the discussion of the Angstrom values (AE) you may know that EAE = BAE +LRAE, as given in Ansmann et al. (JGR, 2002 on ACE-2 observations in Portugal). And that fits very well in your observational cases. However, if the assumed LRAE is height constant, and the BAE is height constant, EAE can only be height constant. But in reality, EAE and LRAE may vary. This should be mentioned. Without the Raman lidar approach you cannot provide information on the

'real world' EAE, extinction, and lidar ratio profiles. They are based on an assumption, and not on measured facts. So it is misleading to show profiles of extinction and EAE without saying that these are just retrieval products heavily controlled by the assumption of a height constant lidar ratio.

A22: As explained in A17, we chose to not use Raman inversion to avoid the distortion of the extinction profile brought by the smoothing. Considering that the PLDRs of the smoke layer do not show noticeable vertical variation (PLDR calculated using the backscatter ratio resulted from Raman inversion, instead of Klett), the particles in the smoke plumes are very likely well mixed so do not have significant variations in the concentration-independent quantities such as PLDR, LR and BAE…

We compared the profiles of backscatter coefficient from Raman inversion and Klett inversion in the two cases presented in the paper, as shown in Figure (2). It can be seen that the backscatter coefficient from Raman and Klett inversion are rather comparable.

It is true that the similarity of the extinction and backscatter coefficient profile is due to the assumption of vertically constant lidar ratio. However, we can be confident that, due to the homogeneity of the smoke layer, the lidar ratio literally does not have significant vertical variations and our assumption is valid.

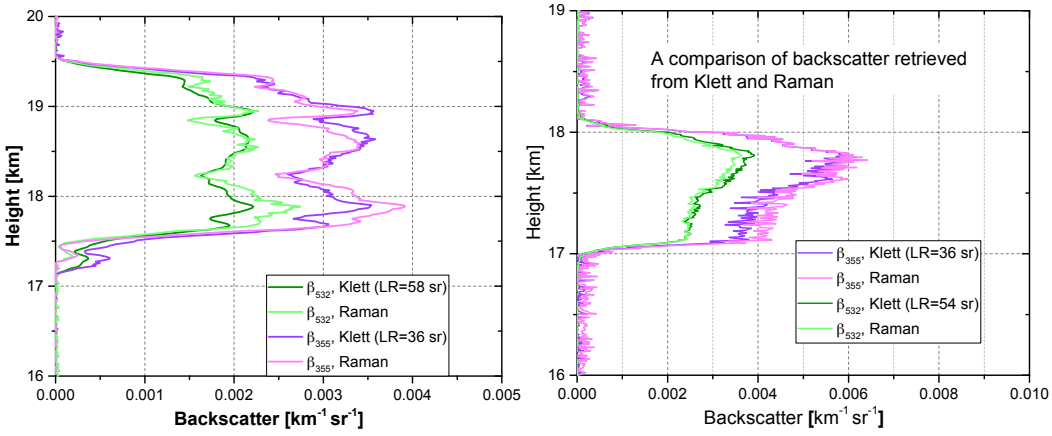

Figure 2. The comparison of backscatter coefficient, (left) 19:20—21:20 UTC, 28 August 2017, Palaiseau and (right) 20:30—00:30 UTC, 24—25 August 2017, Lille

23. *P10, L30: 'The UTLS aerosol layer was between 17 and 18 km'. This is one of the sentences that forced me to ask: Why do you call that an UTLS layers. The layer is clearly in the lower stratosphere.*

A23: Yes it is in the stratosphere. We will correct it to 'lower stratosphere' to be more precise.

24. P11, L13: Figure 10 is questionable and probably not representative to explain the long range transport including transport times. The CALIPSO Figure 6 tells us that the smoke layers were mostly at heights of 14-17 km over North America and the Atlantic, sometimes even below 14 km. And at these heights the wind speeds were much higher than at 17-19 km (in Figure 10). We need more trajectories! Especially for the CALIPSO heights (12-17 km) before we can make conclusions on the travel duration (in the discussion section 5). And one effect makes the use of trajectories difficult: The ascent of the layers from day to day by absorption of sunlight! This is not considered in any trajectory modeling. So trajectories are of limited use here. But 20 days of travel from Canada to Europe? That would be quite new, in view all the papers on Canadian smoke and long range transport. Even Khaykin et al. (2018) writes that the smoke needed 21 days to travel around the globe (at midlatitudes) to be back over Canada again, and that the smoke needed only 10 days or less to reach Europe.

A24: It is true that the time between the first occurrence of the smoke plume generated by pyro-Cbs (12 August) in Canada and our first observations in France (19 August) is approximately about 10 days. However, as we can see in the UVAI maps from OMPS, the smoke plumes were distributed over very large areas and they are transported along

different pathways, moreover the wind fields in different areas are different. So it is not surprising that the plumes transported along different pathways have different transport time and that ~10-day is very likely the fastest transport time.
We can see, from the UVAI map, that on 18 August, the front of the smoke plume has arrived in Europe but the main bulk of smoke plumes was sustained in the east of Canada, where no fire spots were detected. We think that the smoke plumes in this whole event (refer to our observation from 19 August to 02 September) were mostly generated during 11--12 August to 15 August. The smoke plumes distributed over large area and they were then transported to Europe with different transport time.

25. P11, section 4.2.2: Again the question: How trustworthy are the solutions of the inversion method when only based on Klett optical properties, so that the basic information are backscatter profiles? Please comment on that.

A25: Summarizing aforementioned information, the backscatter coefficients from Klett method are rather consistent with from Raman. The The mean extinction coefficients are derived from transmission of the plume, which is also robust and does not suffer from vertical smoothing. We consider the optical data as very trustworthy as input of the inversion. The main error source of the inversion is the use of sphere model, especially for the imaginary part of the complex refractive indices. From our simulation studies we estimate errors of V (volume concentration) and R_{eff} as ±30%, for m_R it is ±0.05 and m_I ±50%. These are typical values and we are not able to evaluate the effect of shape of on retrievals.

Discussion section:

26. P12, L26-28: I have my doubts that one singular event (the major pyrocumulonimbus cluster on 12 August) leads to so many smoke layer that you observed between 24-31 August. To my opinion, layers observed 10 days later maybe linked to the 12 August event, and maybe even layers observed on 24 August. But all other smoke layers later on were most probably triggered by other reasons and causes. And note that the absorbing smoke layers ascended during the travel (because of strong absorption of solar radiation). Khaykin et al. (2018) mentioned, 2-3 km per day during the first days. So layers can easily reach the lower stratosphere after 3 days when initially injected to 8 km height...

A26: As mentioned in **A24**, 10-day is probably the fastest transport time. Due to the large distribution of the plumes and the differences in the wind fields, the plumes are likely to undergo longer transport time.

Let's sort out the time series between 11 and 29 August:

- Emission process: the fire sources (indicated by the fire and thermal anomalies from MODIS) of the smoke plumes are mostly in the Northwest Territories, the Alberta and the British Columbia, large amount of smoke accumulated over the northwest of Canada and propagated easterly. After 15 August, the intensity of the fire activities reduced and the plumes have been transported away from the source region. And on 15—28 August, there were no new plumes with comparable quantity and scale, being generated in the areas with fire spots any more, indicating that the fire activities were weak during this period. We consider that the plumes observed in Europe were mostly generated before 15 August.
- Transport process: the plume that first arrived in Europe came from the 'tail' (see UVAI on 16 August), locating between Canada and the US, of the large bulk of the plume, while the main bulk of the plume still stayed in the north-east of Canada. The main bulk of plume left Canada on 19 August and then propagated to Europe. We can see that on 21 August, the intense plume over central Atlantic has lost 'connection' with the plume over Canada. In the following days, this

intense plume continued propagating to Europe and the transport speed over Europe is much slower. For example, during 25—27 August, the plume hovered over France was changing very slowly. Even on 28, 29 August, the plume changed its shape and intensity, we did not see any new smoke coming from the Canada.

- In addition, the transport time from Canada to Europe and the aging time (between the generation and the observation of the smoke plume) are not the same variable, because of the complicated spatial distribution of the smoke plume. The aging time can be longer than the transport time from Canada to Europe.

As to the ascending trend of the smoke plume, indeed, the plumes tend to ascend when absorbing solar radiation. But we expect that the vertical motion of the wind field should dominate the descending or ascending of the plume.

27. P13, L1: In the discussion of the very large 355 nm particle depol values, please check: There is a corrigendum note to the Burton 2015 paper (you will find it on the ACP page). In this corrigendum note it is stated that the 355 nm depolarization ratios were only 20.5% for the smoke case (and not 24% as erroneously obtained in the beginning of the data analysis and published in Burton et al. (2015) paper). So, again, the 28% you get at 355 nm are really 'outstanding' and must be re-checked.... Find out, for example, how large the impact of the Klett backscatter profile is in the retrieval of the particle depol ratio at 355 nm... by using plus/minus 10% backscatter coefficient profiles.

A27: Please see **A19.**

28. P13, L5-L22: You provide the suggestion (Figure 11) that the depolarization ratio increases with travel time. This is surprising,

because Nisantzi et al. (ACP, 2014, Injection of mineral dust into the free troposphere during fire events observed with polarization lidar at Limassol, Cyprus) find the exact opposite and show that in a figure: Decreasing depolarization ratio with transport time. However, their study is exclusively based on tropospheric smoke. And you combine tropospheric and stratospheric observations in your analysis.

Who is right? Maybe both! But first of all, one has to clearly distinguish aerosols in the troposphere and in the stratosphere. As mentioned, tropospheric as well as stratospheric smoke depolarization ratios are considered in your Figure 11. To my opinion, in this way you compare apples and oranges, and therefore the conclusions maybe wrong, at least are 'dangerous'. In the troposphere, coagulation and interaction with gases and moisture can take place, as you discuss so that aging leads to growing particles. According to measurements they get coated (Dahlkoetter et al, ACP 2014), they get coated with liquid stuff, so they get more and more spherical. And that influences the depolarization ratio. The depol ratio decreases, in accordance with the Haarig et al. (2018) results. In the stratosphere all this is less probable, and coating of soot particle is practically suppressed because the moisture and all the gases are not given in the stratosphere. It seems to be that the particles in the stratosphere remain unchanged during the travel. That is what I see also from the noisy CALIPSO observations in Figure 6 and what is also shown in the Haarig paper. But maybe I am wrong. Please provide us with a convincing explanation why aging leads to an increase in the depolarization ratio!

Disregarding my personal opinion, as a consequence of the statements above and the rather different particle aging processes in the troposphere and stratosphere...: If you want to show Figure 11 than you need to clearly indicate the stratospheric values, may be by very different symbols, e.g., by big open circles. We need a strong contrast between

tropospheric and stratospheric values... The lower values in the Figure are obviously tropospheric depol values (apples) , and the higher ones are stratospheric values (oranges) . Furthermore I have my doubts about transport times of more than 14 days.... The related trajectories are always very uncertain and thus questionable.

Final point: I think the primary goal of the discussion section should focus on the comparison with other findings, especially with Haarig et al. (2018), and also Burton et al. (2015, upper tropospheric smoke case). As mentioned several times, your results are based (to a large fraction) on the use of the Klett method. And this includes the determination of the particle depolarization ratios because the Klett backscatter profiles are needed. This can be a significant reason for deviations, especially in the case of the products at 355nm.

A28: Nisantzi et al, 2014 reported a case of smoke and dust mixtures, the depol decreased with transport time because dust particle deposited with time. This is not our case.

The observations of PLDR in Figure 11 are all above 5 km. Observations below 5 km are filtered out to avoid results in the lower troposphere. But this information is mistakenly not introduced in the manuscript.

CALIPSO data are indeed noisy and suffer from significant error in some cases where the aerosol plumes were not correctly classified. At current stage, we decide to remove Figure 11 and the argument about depolarization ratio increasing with travel time. Still we think it might be a good chance and it is interesting to study smoke aging, but drawing convincing conclusions, much more efforts are needed in investigating and verifying CALIPSO measurements. We will continue this work in the next step.

P13, L23: Regarding the laboratory studies: Miffre et al (2016) used Arizona Test Dust (ATD). This dust is not a natural dust component. It is ‘manufactored’ by a company and ATD particles have rather sharp

edges. As a result, ATD shows larger depol ratios then usual desert dust particles.

Regarding the Jaervinen et al. (2016) study: These authors made their observations by one wavelength (488 nm, and partly at 552 nm) only! ..and not at 355 and 532 nm, as you mention it. But they showed their observations as a function of the size parameter (size mode diameter /wavelength) so that Mamouri and Ansmann (2016) estimated the probable depolarization ratios for 355, 532, and and 1064 nm. The results (depol ratio for fine dust at 355, 532, and 1064 nm derived from the Jaervinen study) are shown in Haarig et al. (2018). Almost all your discussion information on page 13 (L23-34) was discussed in the same way in the papers of Mamouri and Ansmann (2014, 2016). So, please add these papers to your references.

29. P14, L37: Regarding the effective radius (from the lidar inversion retrieval), please compare with Haarig et al. (2018). Is there agreement? Please discuss the comparison.

A29: Comparison and comments are added.

30. P14, L39: Again, please avoid mixing of tropospheric and stratospheric effects of potential particle growth. Müller et al (2007b) focusses on tropospheric smoke only when discussing aging effects.

A30: See **A28**.

31. P15, conclusion section: The results of the paper are summarized only in this section. But concluding remarks are not given. So maybe, create some concluding remarks, some outlook ideas...

A31: Modifications are made.